

INFORMATION TO USERS

This manuscript has been reproduced from the microfilm master. UMI films the text directly from the original or copy submitted. Thus, some thesis and dissertation copies are in typewriter face, while others may be from any type of computer printer.

The quality of this reproduction is dependent upon the quality of the copy submitted. Broken or indistinct print, colored or poor quality illustrations and photographs, print bleedthrough, substandard margins, and improper alignment can adversely affect reproduction.

In the unlikely event that the author did not send UMI a complete manuscript and there are missing pages, these will be noted. Also, if unauthorized copyright material had to be removed, a note will indicate the deletion.

Oversize materials (e.g., maps, drawings, charts) are reproduced by sectioning the original, beginning at the upper left-hand corner and continuing from left to right in equal sections with small overlaps.

Photographs included in the original manuscript have been reproduced xerographically in this copy. Higher quality 6" x 9" black and white photographic prints are available for any photographs or illustrations appearing in this copy for an additional charge. Contact UMI directly to order.

**Bell & Howell Information and Learning
300 North Zeeb Road, Ann Arbor, MI 48106-1346 USA**

UMI[®]
800-521-0600

Automatic Thalamic Labeling for Image Guided Neurosurgery

by

Diego Clonda

**Medical Physics Unit
McGill University, Montreal**

**A thesis submitted to the Faculty of Graduate Studies
and Research in partial fulfillment of the requirements
for the degree of Master of Science.**

©D. Clonda, January 1998.



**National Library
of Canada**

**Acquisitions and
Bibliographic Services**

**395 Wellington Street
Ottawa ON K1A 0N4
Canada**

**Bibliothèque nationale
du Canada**

**Acquisitions et
services bibliographiques**

**395, rue Wellington
Ottawa ON K1A 0N4
Canada**

Your file Votre référence

Our file Notre référence

The author has granted a non-exclusive licence allowing the National Library of Canada to reproduce, loan, distribute or sell copies of this thesis in microform, paper or electronic formats.

The author retains ownership of the copyright in this thesis. Neither the thesis nor substantial extracts from it may be printed or otherwise reproduced without the author's permission.

L'auteur a accordé une licence non exclusive permettant à la Bibliothèque nationale du Canada de reproduire, prêter, distribuer ou vendre des copies de cette thèse sous la forme de microfiche/film, de reproduction sur papier ou sur format électronique.

L'auteur conserve la propriété du droit d'auteur qui protège cette thèse. Ni la thèse ni des extraits substantiels de celle-ci ne doivent être imprimés ou autrement reproduits sans son autorisation.

0-612-44150-4

Contents

List of Figures	vii
Acknowledgments	viii
Abstract	ix
Résumé	x
Contributions	xi
List of Symbols and Abbreviations	xii
Preface	xiv
Introduction	xvi
1 Historical background	1
1.1 Stereotaxy	1
1.1.1 Historical review	2
1.1.2 Terminology	2
1.2 Parkinson's disease	3

1.2.1	Tremor mechanism	4
1.2.2	Conditions for surgery	5
1.2.3	Site of lesion	6
1.2.4	Lesioning	8
1.2.5	Drawbacks	9
2	Methodology used for the Parkinson's surgery	10
2.1	Image Guided Neurosurgery	10
2.2	Imaging modalities	11
2.2.1	Ventriculography	11
2.2.2	Magnetic Resonance Imaging	12
2.3	The image format	13
2.4	Surgical tools	15
2.4.1	Stereotactic frame	15
2.4.2	Stimulator	18
2.4.3	Leukotome	18
2.5	Procedure	20
2.6	Lesion planning	21
3	Atlas creation	23
3.1	The atlas data set	23
3.2	The computerized atlas	26
3.2.1	Digitization	26
3.2.2	Alignment	27

3.3	The three-dimensional atlas	31
3.3.1	The vector format	31
3.3.2	Interpolation	34
3.3.3	Image format	36
3.3.4	Drawbacks	37
3.3.5	Atlas content	40
3.4	Segmentation model	43
3.4.1	Model MRI	43
3.4.2	Manual tagging	44
3.4.3	Transformation	47
4	Registration	49
4.1	Introduction	49
4.2	Linear transformation	51
4.2.1	The transformation	51
4.2.2	The algorithm approach	52
4.2.3	Features	53
4.2.4	Procedure	54
4.3	Non-linear transformation	57
4.3.1	The transformation	57
4.3.2	The algorithm approach	58
4.3.3	Procedure	59
5	Imaging platform	62

5.1	Navigation	63
5.2	3-D rendering	64
5.2.1	Volume rendering	64
5.2.2	Surface rendering	65
5.2.3	Stereoscopic view	66
5.3	Surgery oriented tools	67
5.3.1	Modeling of the surgical tools	67
5.3.2	Lesion planning	69
5.3.3	MR to frame space	71
5.3.4	Annotations	71
6	Conclusion and Future Work	72
6.1	Conclusion	72
6.2	Future Work	73
	Bibliography	74

List of Figures

1.1	The genesis of tremors	5
1.2	Site of the lesion.	7
2.1	Ventriculograms.	11
2.2	Axial view of a patient's brain MR.	13
2.3	MINC transformation.	14
2.4	The OBT stereotactic frame.	16
2.5	The stereotactic frame with the fiducial markers.	17
2.6	The stereotactic frame with the surgical arc system.	18
2.7	The stimulator.	19
2.8	The leukotome.	20
2.9	The off-axis extent of the lesion.	22
3.1	Mid sagittal view of the right hemisphere of brain LXXVIII [29] showing axial slices.	24
3.2	The cryotome and film data-sets at the -1.5 mm section [29].	25
3.3	The reference point for the alignment.	28
3.4	The origin point of the (x, y) axes.	29
3.5	The three views of the stacked cryotome volume.	31

3.6	Transformation into vector format.	33
3.7	The interpolation from the vector contours.	35
3.8	From vector format to voxel format.	36
3.9	Coronal view of the atlas.	38
3.10	Left 3-D view of the putamen.	40
3.11	An axial view of the atlas.	42
3.12	The model brain MRI (SuperBrain).	44
3.13	The tagging points for the -1.5 mm section.	46
4.1	The features volumes.	55
4.2	The lattice sampling.	60
5.1	The imaging platform	63
5.2	Grey matter weighted volume rendering view of the SuperBrain.	65
5.3	A 3-D view of the thalamic nuclei.	66
5.4	The leukotome in the planar views.	67
5.5	The leukotome with 3-D objects.	68
5.6	The perpendicular trajectory view.	69
5.7	The lesion planning tool.	70

Acknowledgments

I wish to thank Dr. Abbas Sadikot and my supervisors Drs. Alan Evans and Terry Peters for providing the initial ideas for this master project. I am particularly grateful to Terry for his constant academic support and to Abbas for his close collaboration and interaction in the development of the project as well as to both of them for being a great source of motivation with their everlasting enthusiasm.

I sincerely thank Philippe St-Jean for his close collaboration throughout the course of this work, for his inexhaustible enthusiasm and for always pushing me to work harder.

I would like to thank the people of the Brain Imaging Centre for their help and for providing the great software environment. In particular I am very grateful to Dr. Louis Collins for his ANIMAL registration tool and to Dr. Noor Kabani for having kindly performed the manual tagging of the atlas onto the model MRI.

A special thank to everybody of the NeuroImaging group for their general help and for providing precious advice, in particular to Roch Comeau for technical support on all software related things and for his help at the beginning of this work, especially with the scanning.

Finally I sincerely thank my family, my brother Valerian Clonda and my parents Georges Clonda and Begonia Peñacoba for their everlasting love and support.

I would like to acknowledge the financial support of the NSERC (PGS-A) throughout the course of this work.

Abstract

In the treatment of Parkinson's disease some cases require the ablation of a specific region in the basal ganglia. The accurate localization of this region inside the patient's brain is essential and because direct visual anatomical information for such deep brain structures is not available, the surgeon has to rely on other sources of information such as MRI, CT and x-ray of the patient's brain. However these imaging techniques do not provide sufficient anatomical information, requiring the use of a subcortical brain atlas book to assist in the localization of the different structures. This way of proceeding is cumbersome and results in a certain lack of accuracy in the localization of the different brain structures.

We developed a method that aids the surgeon to obtain the sufficient anatomical information in a simpler and more accurate manner. We provide him with a segmentation of the patient's MRI scan based on the Schaltenbrand and Wahren subcortical atlas. To achieve such segmentation a volumetric version of the atlas was obtained and was then mapped to a model brain MRI using landmark matching. Using an automated tool for the three-dimensional registration of two MRI volumes the deformation transformation between the model brain MRI and the patient's brain MRI was obtained. By applying this same transformation to the volumetric atlas, we obtain a superposition of a volumetric subcortical atlas onto the MRI of the patient's brain in the stereotactic space. This method results in a more accurate localization of the surgical lesion, thus reducing the number of additional interventions which are often necessary when the results of the first procedure are shown to be unsatisfactory. The whole guidance system is now used routinely at the Montreal Neurological Institute and is part of the standard surgical procedure.

Résumé

Dans certains cas, il est nécessaire de recourir à une intervention chirurgicale pour traiter adéquatement les patients atteints de la maladie de Parkinson. La chirurgie consiste à faire une lésion à une petite structure du cerveau située dans la région du thalamus, et demande une localisation précise afin d'éviter d'endommager les structures avoisinantes. Étant donné que cette région se situe au centre du cerveau, les structures ne sont pas visibles à l'oeil nu. Le chirurgien doit donc se référer à des images provenant de l'IRM, du CT et des rayons X. Malheureusement, ces images contiennent assez peu de détails anatomiques dans cette région du cerveau, rendant nécessaire l'utilisation conjointe d'un atlas afin d'obtenir une localisation adéquate. Une telle utilisation de l'atlas ne permet qu'une localisation approximative de la région à exciser. Nous avons développé un système qui permet au chirurgien d'avoir accès à cette information anatomique de façon plus simple et plus précise grâce à une segmentation de l'IRM du patient, basée sur l'atlas thalamique de Schaltenbrand et Wahren. Pour obtenir une telle segmentation, une version tri-dimensionnelle de l'atlas a tout d'abord été créée. Dans le but de profiter d'un outil de recalage déjà existant, cette version a ensuite été déformée manuellement afin qu'elle corresponde à un modèle IRM. La déformation de l'IRM du modèle à celui du patient s'effectue ensuite de façon automatisée en utilisant l'outil permettant le recalage tri-dimensionnel et non-linéaire entre deux volumes IRM. Ce système a été incorporé à la procédure chirurgicale courante et il est maintenant utilisé de façon régulière à l'Institut Neurologique de Montréal pour le traitement de la maladie de Parkinson. Un tel système devrait permettre une localisation plus précise des différentes structures dans la région du thalamus et ainsi permettre de mieux contrôler l'étendue de la lésion.

Contributions

Diego Clonda, P. St-Jean, A. Sadikot, T.M. Peters, A.C. Evans. Automatic labeling of the patient's brain with a subcortical atlas in image guided neurosurgery. In *Proceedings of the Canadian Organization of Medical Physicists*, pages 209-211, 1997.

Philippe St-Jean, D. Clonda, A. Sadikot, A. Evans and T. Peters. Computer guidance for thalamotomy and pallidotomy. In *Proceedings of the Canadian Organization of Medical Physicists*, pages 146-148, 1997.

Philippe St-Jean, Reza Kasrai, Diego Clonda, Abbas F. Sadikot, Alan C. Evans, and T. Peters. Interactive 3-dimensional visualization tools for stereotactic atlas-based functional neurosurgery. In *Proceedings of the SPIE*, SPIE 98 Medical Imaging.

List of Symbols and Abbreviations

2-D	Two-Dimensional
3-D	Three-Dimensional
AC	Anterior Commissure
ANIMAL	Automatic Nonlinear Image Matching and Anatomical Labeling
C, C++	C and C++ computer languages
Ce	Ventro caudal nucleus
CT	Computed Tomography
DSA	Digital Subtraction Angiography
FFT	Fast Fourier transform
FWHM	Full width at half maximum
ICBM	International Consortium on Brain Mapping
IGNS	Image-Guided Neurosurgery
MINC	Medical Image Net CDF
MNI	Montreal Neurological Institute
MRI	Magnetic Resonance Imaging (or Images)
OBT	Olivier-Bertrand-Tipal Stereotactic Frame
PC	Posterior Commissure
V	Volt
Vci	Ventralis centralis internus nucleus
Vce	Ventralis centralis externus nucleus



Vim

VIPER

Ventralis intermedius motor nucleus

Visual Integration Platform for Enhanced Reality

Preface

The work presented in this thesis is part of a whole project undertaken jointly by Philippe St-Jean and the author. It consisted of creating a volumetric version of the Schaltenbrand and Wahrenthalamic atlas [29] and mapping it to a model MRI. Then by using a MRI-to-MRI registration tool, the model MRI, and thus the atlas, was mapped onto the patient brain. The appropriate tools for the visualization of the atlas over the patient's MRI along with different other tools for an optimal guidance and planning were also developed. The author was responsible for the creation and the registration of the atlas on the patient's MRI while the implementation in the operating room in terms of visualization and guiding tools was carried out by Philippe St-Jean.

A first volumetric version of the atlas was obtained from the joint work of Philippe St-Jean and the author. The scanning, contour extraction, interpolation and definition of the 3-D regions were carried out by both of them.

The second and final, more refined version of the atlas was then obtained by the author. In that version, new regions were added and some alignment corrections were made.

The tagging of the volumetric atlas onto the model MRI was performed for each of the two atlas versions by Dr. Noor Kabani.

For the registration from the model MRI to the patient's MRI, we used the ANIMAL non-linear registration tool developed at the MNI by Dr. Louis Collins. At the time of writing this thesis, no modification specific to our needs was made and the generic version of this tool was being used.

For the visualization both in the operating room and for the planning, we use the VIPER

imaging platform. This platform has been developed in the NeuroImaging laboratory by Robert Flantz, Reza Kasrai, Philippe St-Jean and Mike Sinasac.

The specific features in VIPER particular to the thalamotomies as well as lesion planning and lesion modeling tools were developed by Philippe St-Jean.

Introduction

In the regular surgical procedure for the treatment of Parkinson's disease, ventriculography is used to localize the main brain structures (AC-PC line and mid-sagittal plane). Then by using the MR images and the atlas book, the surgeon is able to localize more or less the particular structures important for surgery (i.e. globus pallidus, thalamic nuclei, etc...). This way of proceeding is cumbersome (turning the atlas pages) and gives only an approximate localization, requiring a fairly long stimulation procedure. The tool presented in this thesis will, we believe, greatly help the surgeon to localize the different structures in the stereotactic space. The benefits are a rapid and fairly accurate localization of the brain structures from the computer's images, thus reducing the stimulation time, but also a 3-D visualization of the brain regions, resulting in a more adequate selection of the target volume.

The tool is based on a labeling of the patient's brain MRI according to the Schaltenbrand and Wahren atlas [29] along with the use of a visualization platform with specific features to help the surgeon with the planning as well as for guidance during the operation. The labeling is achieved by registering a segmented model MRI onto the patient's brain MRI and thus obtaining a segmentation of the latter. The procedure is completely automated and gives fairly accurate results.

In chapter 1, the stereotactic surgical procedure will be briefly explained followed by a description of certain notions regarding the Parkinson's disease and its surgical treatment.

Chapter 2 will present the context in which the tools we developed are meant to be used. The overall surgical procedure, the different tools used, the imaging modalities as well as the software environment will be described in this chapter.

Chapter 3 is devoted to the atlas itself. Details will be given about the original information contained in the atlas book, the creation of the volumetric version and the mapping onto the model MRI.

The non-linear registration from the model MRI to the patient's MRI will be the subject of chapter 4. A description of the method, the different steps involved in the algorithm as well as the features used will be made.

Finally, chapter 5 will focus on the imaging platform used in the operating room to display the thalamic atlas. Its general features, as well as the specific tools developed for our particular case of thalamic surgery will be described here.

Chapter 1

Historical background

1.1 Stereotaxy

Stereotaxy is one of the commonly used techniques available for neurosurgery. It involves applying a 3-D coordinate system to the brain of the patient in order to perform a precise surgical task at the surface of, or inside the brain. The requirements for this type of operation are a very precise and accurate handling and localization of the surgical tools along with a reproducibility of the procedure. This is achieved by fixing a rigid frame to the head of the patient and tightly attaching the surgical tools to it. This frame defines the stereotactic space, which is used to localize the different brain structures. By imaging the brain with the frame in place, for instance with X-rays, CT or MRI scans, we can relate some internal anatomical landmarks to the frame coordinate system. Stereotaxy has been used for surgical procedures requiring high precision localization of deep brain structures, like in the lesioning of thalamic nuclei for Parkinson's disease, the placement of radioactive seeds in intracavitary brachytherapy or locating the target during treatment with high-energy ionizing radiation beams.

1.1.1 Historical review

Stereotaxy first appeared in 1906 when Horsley and Clarke used a 3-D coordinate system for their research on the function of the cerebellum. The experiment was performed on monkeys with a rigid frame fixed to the head to serve as a support for a more accurate positioning of the electrodes. The coordinate system was defined from external anatomical landmarks (skull) and in 1908 they published the first stereotactic brain atlas (monkeys) [16]. In 1947 Spiegel and Wycis presented the first stereotactic operation performed on humans [32]. Radiographic images of the brain (ventriculography) were used to define the coordinate system with respect to internal cerebral structures, thus greatly increasing the accuracy of the procedure. They published the first human stereotactic brain atlas in 1952 [31]. This technique became very popular from the fifties onward, especially in the treatment of Parkinson's disease and a few improvements were made, mainly on the stereotactic frame, allowing for more versatility in the positioning of the surgical tools. The advent in 1969 of a new drug for Parkinson's disease, the L-dopa, marked a serious decline in the popularity of stereotaxy (see section 1.2). However the arrival of computed tomography (CT) in 1973 [17] shed a new light on this field and by 1976 [4] the two techniques were combined together. CT not only provided more anatomical information of the brain but it allowed the 3-D coordinate system to be defined directly from the frame itself rather than from some anatomical landmarks on the skull and the brain. In the following years a lot of research efforts were made to improve the compatibility of the frame with CT, and also particularly on the computer software that was used for the localization of the target in the stereotactic space. The advent of MRI proved also to be very useful to stereotaxy, with the much higher soft tissue (brain) contrast it provides compared to CT or ventriculography.

1.1.2 Terminology

Special attention should be paid to the terminology used since there might be some confusion between the two terms *stereotaxic* and *stereotactic*. The root *stereo* comes from the Greek meaning "solid" or "three-dimensional", the word *taxic* means "arrangement", "system" while *tactic* means "to touch". This question was addressed officially in 1973 and it was concluded that the

word stereotactic describes more adequately the idea of stereotaxy, giving the feeling of being able to touch the deep brain structures. We have adopted the convention of using *stereotactic* in reference to surgical procedures, and *stereotaxic* when referring to “standard” space. The word stereotaxic should be used to describe a standard space where different brains are put together for their study, for instance the Talairach stereotaxic space [34].

1.2 Parkinson’s disease

The debut of the surgical treatment of Parkinsonian patients is closely related to the first stereotactic procedure performed on human brain in 1947 by Spiegel et al. [32]. A few years earlier, Meyers [24] had shown that rigidity and tremor symptoms caused by Parkinson’s disease were considerably improved by the excision of part of the caudate nucleus and the ansa lenticularis. It marked the beginning of intensive research on the surgical treatment of dyskinesia with the principal lesioning regions being the globus pallidus [9, 19, 33] and later the nucleus ventralis lateralis [14]. The excision of these, as well as other basal ganglia structures appeared to be very effective for the treatment of motor disorders such as the tremor and rigidity involved in Parkinson’s disease. This enthusiasm was greatly slowed down by the advent in the seventies of a new drug, L-dopa. Even though this drug was mostly effective in alleviating the rigidity problem, leaving the tremors (when present) with little or no improvement, the overall results were so impressive that surgery was only performed on rare occasions. The use of stereotactic intervention was left for patients who did not respond to the drug or for those who presented persistent tremor problems (see section 1.2.2). Patients afflicted by Parkinson’s disease may also present disorders other than rigidity and tremor, for instance bradykinesia, impaired gait, dysphasia or ocular disturbances, however these symptoms are less likely to be substantially improved by a surgical procedure [35].

Tremor associated with Parkinson’s disease is believed to be caused by a dysfunction of the extrapyramidal motor system (basal ganglia). It comes in the form of a low frequency tremor, varying from 2 to 7 but generally of 4–5 oscillations/sec, usually exhibiting a fairly rhythmic,

constant frequency, behavior [36]. It involves the muscles at the extremities of the limbs, most often the arm, contracting the thumb and the fingers in a “pill-rolling” fashion, and in the leg, resulting in a tapping motion of the foot. In some cases, facial, jaw or even lingual muscles are stricken by the tremors. The shaking is usually unilateral, but can sometimes evolve to afflict both sides. Most often the tremor is present when the limb is at rest and can completely disappear during intentional movements. It should also be noted that the patient is not afflicted during sleep and that both emotional or physical stress can increase the strength of the tremors.

1.2.1 Tremor mechanism

There are still many unknown details regarding the exact mechanism responsible for the genesis of tremors in Parkinson’s disease. Microelectrode recordings have shown the presence of rhythmic burst discharges in the nucleus ventralis intermedius (Vim) [1, 5, 5, 13]. These discharges come in trains of three or four spikes and it can be demonstrated that they exhibit a direct temporal correspondence with the contraction of the muscle associated with the shaking [25]. The presence of these bursts is very well localized to the Vim, especially in its ventral region.

However, the exact mechanism leading to the burst genesis is still uncertain. The most likely hypothesis is that partial deafferentation to the Vim is responsible for this rhythmic activity [3]. This signal is then sent to the motor cortex, resulting in the rapid contraction of the muscles involved in the tremor. Destruction in the Vim of the efferents coming from the pallidus improved the rigidity problem while the created lesion, involving the cerebellar efferents, stopped the tremors [30].

Muscle tone plays another important aspect of the nature of Parkinsonian tremor. A higher muscular tone tends to increase the frequency of the tremor, as well as regularizing its rhythm. In that sense, Parkinsonian patients treated with L-dopa who benefit from a relief of rigidity, but not of the tremor, will see the shaking rhythm become less regular and with usually a lower frequency. The influence of the muscle tone on the tremor mechanism is believed to be exerted via the anterior horn of the spinal cord, where the spinal reflex loop takes place. The signal is then sent to the stretch receptor area of the Vim where it can interact with spontaneous burst

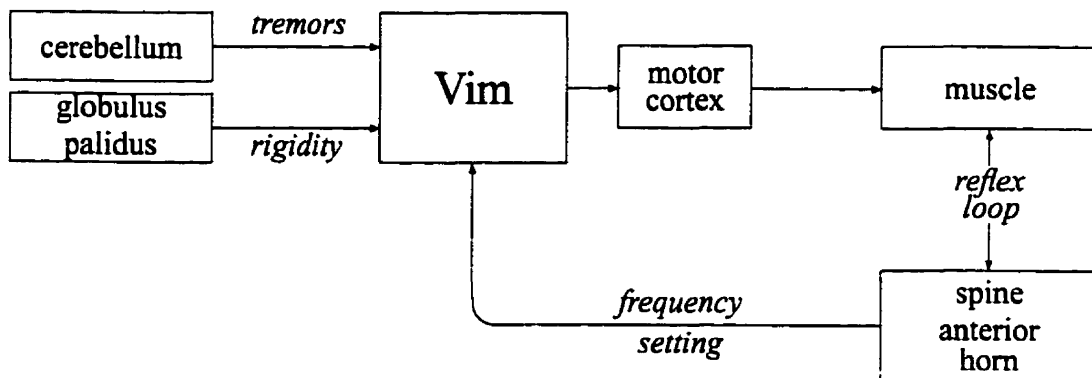


Figure 1.1: The genesis of tremors

The different elements involved with the tremors in Parkinson's disease.

discharges [25]. While the Vim is responsible for the generation of the bursts, the reflex loop sets the rhythm (and frequency) of the tremor. Fig. 1.1 illustrates these different aspects of the tremor mechanism.

1.2.2 Conditions for surgery

Surgery is left for Parkinsonian patients who have not responded to L-dopa or who still present a strong rigidity and or tremor problem after the drug treatment. Ideally the patient should present symptoms predominantly on one side since individuals with bilateral symptoms are less likely to benefit from substantial results after the surgery. Moreover, the patient should be mentally alert since a certain intellectual deterioration may follow surgery, and the blood pressure must be sufficiently low since the risk of hemorrhage following the intervention is high. In ideal conditions (unilateral, mentally alert and normotensive), the patients have a better than 80% chance of being almost completely relieved of their symptoms without any side effects from the operation.

1.2.3 Site of lesion

The proposed area of the brain where the lesion should be performed varies depending on the surgeon as well as on the disorders that need to be treated [25, 35]. The target area is usually in the vicinity of the nucleus ventralis intermedius (Vim). For tremors, the electrical flow from the cerebellum is involved, therefore the lesion is performed on the posterior part of the Vim, i.e. the area of cerebellar projections [30]. For rigidity the lesion is performed more anteriorly in Vim in order to destroy the pallidal efferents: the lesion might even include a part of the nucleus ventralis lateralis (Vl), anterior to the Vim, or might be extended to include some projection fibers of the internal capsule. The lesion can be also performed in the globus pallidus itself. With this in mind, the exact location and size of the lesion depends on the surgeon and may be modified in the light of new studies. In our situation at the MNI, a lesion is performed on the Vim when tremors are predominant while to alleviate rigidity problems, the target area is the internal globus pallidus (see Fig. 1.2).

The localization of the excision region is made using different techniques. Since direct visualization of the deep brain structures is not available during surgery, a rough localization is made using imaging modalities like CT scan, X-rays and more recently MRI scans, and with the help of a thalamic atlas. A more accurate localization is achieved using techniques such as electrical stimulation and microelectrode recording.

By inserting a probe with a microelectrode at its tip in the thalamic area, it is possible to “listen” to the electrical activity of the region. Since different regions produce different signals, in particular the Vim with its characteristic bursts, it is possible to obtain an accurate localization of the tip of the electrode according to the recorded signal. In the stimulation process, instead of listening, electrical impulses are sent from the tip of the probe. According to the response of the patient, who is awake during the operation, (e.g. he is aware of contraction of a muscle, pain sensation, visual artifacts, etc...), it is possible to localize the different motor or sensory areas and thus avoid lesioning critical areas like the internal capsule or the optic tract.

Before reaching this stage of the procedure, the surgeon needs to get a general feeling of the positioning of the different structures in the brain. This is achieved by imaging the brain in

the stereotactic space with a ventriculogram (X-rays with a contrast agent injected in the ventricles), CT scans or more recently with MRI. These images provide some anatomical insight, for instance the position of the mid-sagittal plane and the AC-PC line. Then with the help of the Schaltenbrand and Wahren atlas book [29] (see section 3.1), the surgeon can approximately localize the particular structures and get an appreciation of their relative positions providing some guidance while performing the accurate localization using stimulation and electrical recording. Using this approach, the atlas gives only a rough idea of the position of the structures. The tool I propose in this thesis provides means of labeling the patient's brain according to the atlas in the stereotactic space, giving a much more accurate localization of the structures. It is anticipated that this approach will greatly speed up the localization of structures, leaving the stimulation process only as a confirmation of the exact position of the region to excise; it will also help the surgeon to visualize the three-dimensional shapes of the different structures in the vicinity of the proposed surgery.

1.2.4 Lesioning

Different techniques are available for creating lesions in the desired region. Here at the MNI, the surgery is performed using a sort of mechanical knife called the leukotome. This type of instrument makes fairly precise lesions with sharp edges, and is free of complications. For more details on this technique see Section 2.4.3. Other approaches include injection, thermogenic and cryogenic techniques [25]. In the injection method, a corrosive compound is injected at the site of the lesion, however even with a special care some diffusion might occur, especially along the trajectory of the probe, causing unwanted damage. The lesion can also be obtained by heating the region to about 60°C until some necrosis is achieved, using a high frequency (2 MHz) generator coupled to an electrode. This results in a core of coagulated dead cells surrounded by a region with only partial damage and does not result in the desired clear-cut edge for the lesion. Moreover, the coagulated core might stick to the probe, which when removed could provoke serious hemorrhage. Alternatively the tip of the probe could be frozen to about -160°C. It presents fewer drawbacks than heating the probe but requires a careful control of the temperature.

1.2.5 Drawbacks

This type of surgery is relatively risk free and results in over 80% of the cases in an immediate and complete or almost complete alleviation of the rigidity or tremor symptoms caused by the Parkinson's disease. If the localization of the lesion area is performed carefully, the patient will not suffer from any loss of motor or sensory function. There however might be some minor side effects to the operation; the patient might suffer from a slight intellectual deterioration, especially with older people; and, some temporary dysphasia might be present in the weeks following the intervention. The danger of causing a hemorrhage in the brain during the insertion of the surgical probe is also present, having serious repercussions on the health of the patient.

Chapter 2

Methodology used for the Parkinson's surgery

2.1 Image Guided Neurosurgery

In many instances of surgery in general, and neurosurgery in particular, direct visualization of the lesion is not always possible or adequate. It is therefore often necessary to use images from a variety of modalities to guide the surgical procedure. The purpose of these images is to provide anatomical (CT, MRI and ultrasound) and arterial (DSA) information and also some insight about the evolution of the situation (video image of the cortex and surface deformation tools). Computers play a central role in image guided neurosurgery (IGNS) not only for the viewing of these images but also their editing, for instance in the extraction of surfaces and volume deformation. With the help of a visualization platform, like the VIPER system developed here by the NeuroImaging group and described in greater detail in Chapter 5, the surgeon is able to navigate throughout the brain volume, obtain information from the different modalities at the same time and visualize stereoscopically 3-D surfaces and volumes of the brain. All this information is very useful for both planning and guidance during the operation, allowing the surgeon to perform more accurately and quickly. With the availability now of powerful low price computers, permitting us to perform tasks that were unimaginable before, imaging is destined to play an ever

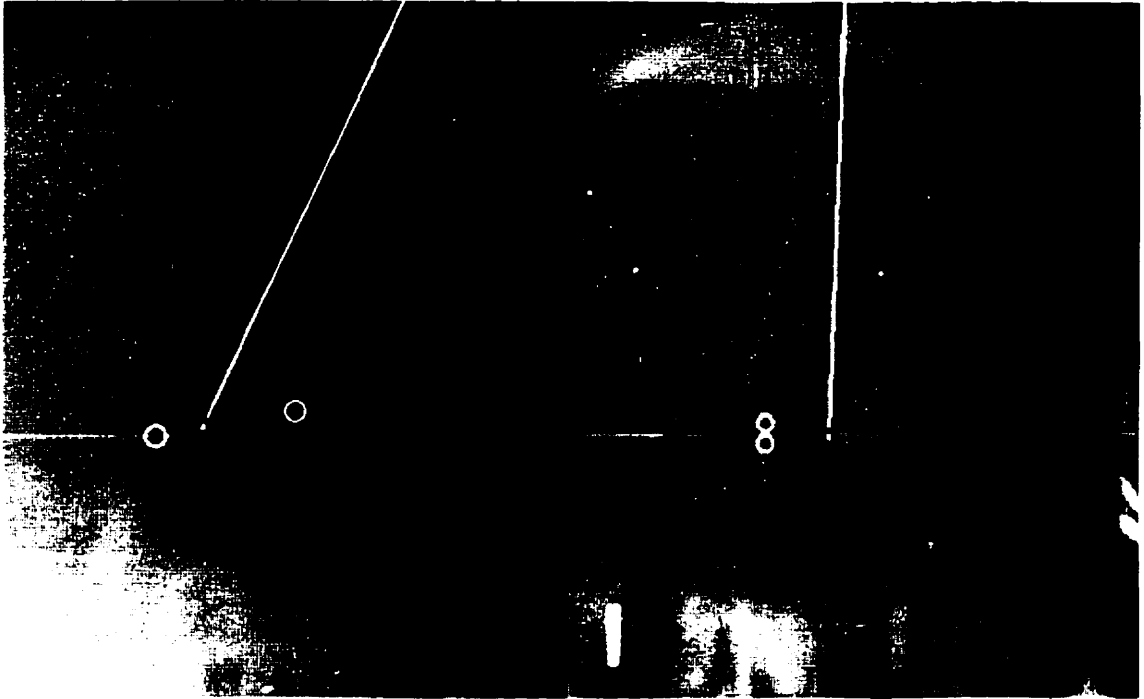


Figure 2.1: Ventriculograms.

Lateral and antero-posterior ventriculograms with the AC and PC (white) and target (black) location

more and more important role in neurosurgery.

2.2 Imaging modalities

In the surgical procedure for the treatment of the Parkinson's disease performed at the MNI, the two modalities used to image the brain are ventriculography and MRI scans.

2.2.1 Ventriculography

Ventriculography is performed in the first stage of the operation with the stereotactic frame fixed to the head and a small opening made on the top of the skull. By inserting a needle through the opening (burr-hole), a contrast agent is injected in the third ventricle; X-rays are then taken in both lateral and postero-anterior orientations, as illustrated in Fig. 2.1. Since the radiograph

is taken with the frame on, we can readily associate the anatomical information to the spatial coordinate system defined by the frame. However, even with the contrast agent, the anatomical details available on a ventriculogram are limited; therefore, these images serve mainly to identify the AC-PC line and the approximate location of target. Even though this procedure involves some risks, particularly in the insertion of the needle where care should be taken not to cut a blood vessel, this step is essential since it gives a geometrically accurate (free of spatial distortion) image more accurate than that obtained with MR.

2.2.2 Magnetic Resonance Imaging

A Philips Gyroscan MRI with a 1.5 Tesla magnet is used to acquire the MR images. A pre-operative scan is performed the week before the operation without the stereotactic frame, allowing the scan to be acquired with the head coil. The head coil is a special device used when imaging small volumes (like the head) giving a better quality image. After the frame is fixed to the head (usually the day before surgery), a second scan is taken; unfortunately, since the head coil of the MR scanner is too small to be used along with the frame, the scan is acquired with the normal body coil, resulting in a lower quality image. A T_1 weighted sequence with a good grey to white matter contrast is used and because of time constraints (no more than 20 min or even less depending on the patient's condition) a slice thickness of 1.5 mm with a lateral resolution of around 1mm is usually taken. A picture of such a MR scan is shown in Fig. 2.2. Since the scan is performed with the frame on the head, each image voxel can be addressed by its stereotactic frame coordinate. This feature, combined with the high degree of anatomical detail available on the image, makes MRI a very useful modality for the planning and guidance in neurosurgery. However because geometrical distortions are still important, it cannot be used alone for an accurate localization of the target. Presently some research is being performed on distortion correction algorithms and on CT based correction (the MR volume is deformed according to the CT scan of the patient's head). This might eventually lead to sufficiently accurate MR scans, obviating the need for ventriculography. MRI has the advantage that it provides a very high anatomical contrast of the brain (much more than CT) and that the procedure is very safe since no radiation

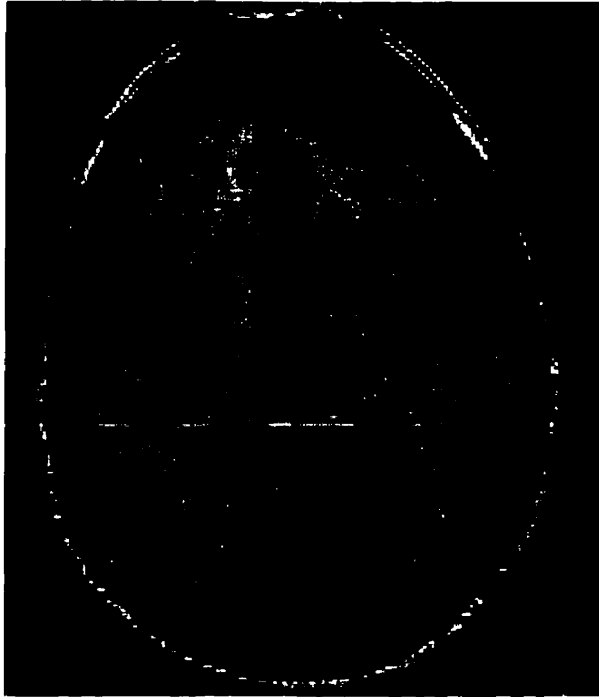


Figure 2.2: Axial view of a patient's brain MR.

dose is given to the patient and no invasive techniques, such as the needle insertion, are used.

2.3 The image format

For most of the editing and rendering of the images we use the MINC (Medical Image Net CDF) format. This format is standard throughout the MNI and provides interesting features. The image data are stored in a “volume” having from 1 to 5 dimensions but usually 3 (3-D volume). Each location in the volume is assigned both voxel (V_1, V_2, V_3) and world (W_1, W_2, W_3) coordinates. The voxel coordinates correspond to the grid sampling position within the volume (i.e. at each integral voxel value between 0 and the volume size an image value is stored). The world coordinates correspond to the “real” location of that point, for instance the millimetric position with respect to a reference frame. Voxel and world coordinates are related via a full (12 parameters: translation, rotation, scaling and axis shearing) affine linear transformation $S : V = S.W$ (i.e. S is the sampling transformation). The volume can be resampled along a new grid pat-

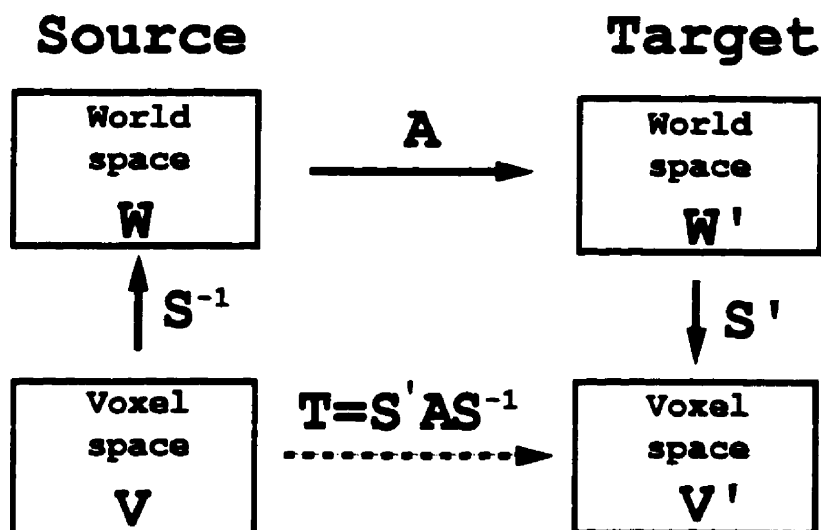


Figure 2.3: MINC transformation.

The different coordinate systems and the transformation relating them.

tern by changing the sampling transformation: $V' = S'.W \Rightarrow V' = S'.S^{-1}.V$. During the resampling, data values are interpolated from neighboring voxels using a specified algorithm (e.g. linear, tricubic, etc...). When a volume undergoes a deformation, as in registration for instance, a transformation A , either linear or non-linear, will be applied to its world coordinates $W' = A.W$. The resulting voxel-to-voxel transformation T ($V' = T.V$) will be given by $T = S'.A.S^{-1}$ ($V' = S'.W' \Rightarrow V' = S'.A.W \Rightarrow V' = S'.A.S^{-1}.V$). A diagram illustrating these concepts is shown in Fig. 2.3. Two of the most important operations performed on image volumes in this work is segmentation and the registration. The registration of one volume onto another consists of calculating within certain constraints (linear, non-linear, etc...) the transformation that will result in the best superposition of the two volumes together; superposition is always performed using world coordinates. The segmentation of a region within an image is the delineation of the extent of each region along with their identification [8].

2.4 Surgical tools

The principal surgical tools used at the MNI for the surgical treatment of the Parkinson's disease are the stereotactic frame, with its different attachment devices, the leukotome and the stimulator.

2.4.1 Stereotactic frame

The stereotactic frame used for the thalamotomy was developed by Olivier-Bertrand-Tipal (OBT) and is closely related to that conceived by Leksell [20, 21, 22]. The frame is fixed to the head of the patient during the first stage of the operation where shallow holes are drilled into the patient's skull under a local anesthesia. The frame is then fixed by fitting carbon fibre pins into the holes and tightly locking them to its structure. Once attached, the frame is relatively painless to wear. The coordinate system is defined by the frame itself, with the axes being along the frame poles. The origin is defined as the midpoint of the anterior section of the base with the X -axis running anterior to posterior, the Y -axis running inferior to superior and the Z -axis running from right to left.

The frame, shown in Fig. 2.4, is composed of a base-ring to which four vertical rigid plastic posts are attached and joined at the top by two plastic and two aluminum bars. The base is made of three aluminum and one plastic sections to avoid forming a closed conducting loop that would cause serious problems during the MRI scanning. The frame is equipped with interchangeable plates, specific to each imaging modality, containing fiducial markers that are used as landmarks on the images to associate them with their coordinates in stereotactic space (see Fig. 2.5). Other devices include an arc system used to attach the surgical tools (leukotome, stimulator, etc...) to the frame. The arc allows the selection of two angles (the declination: antero-posterior and the azimuth: left-right) for complete freedom in the trajectory selection. The frame with the attachment arc is shown in Fig. 2.6.

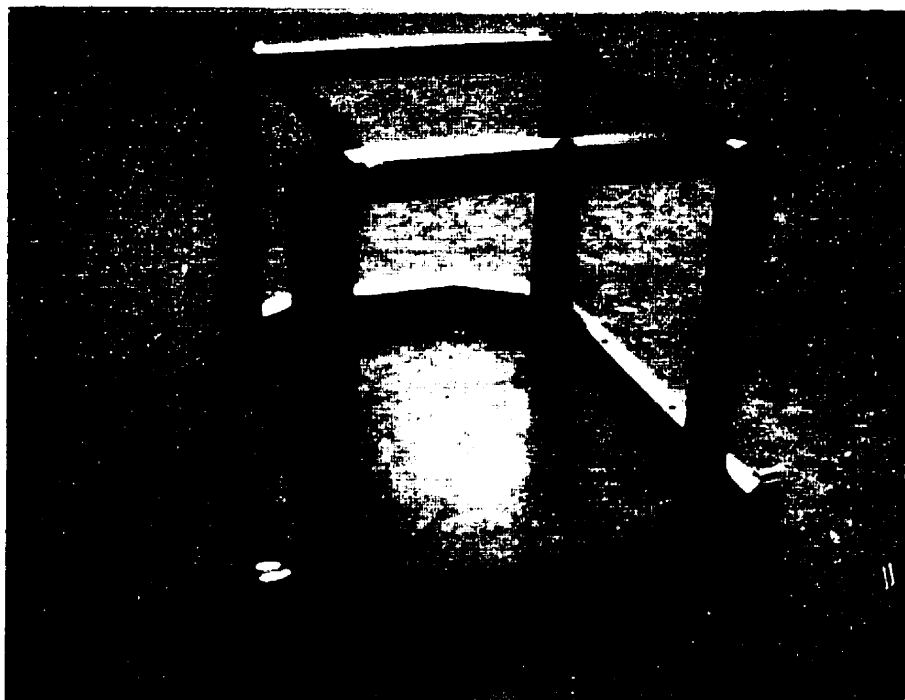


Figure 2.4: The OBT stereotactic frame.

A frontal view of the stereotactic frame.

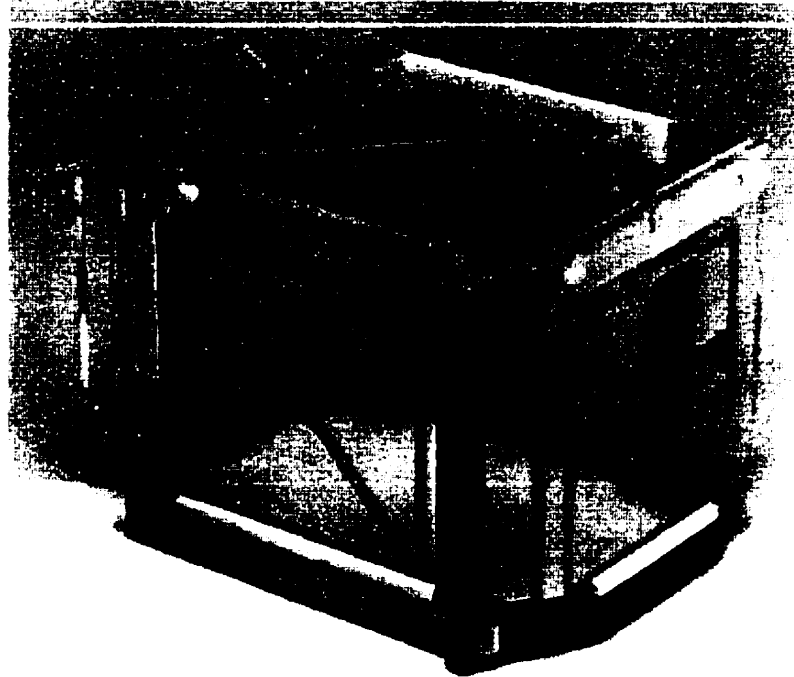


Figure 2.5: The stereotactic frame with the fiducial markers.
The frame with the fiducial marker plates for CT on the anterior, lateral and superior faces along with the plate for MRI on the posterior face.

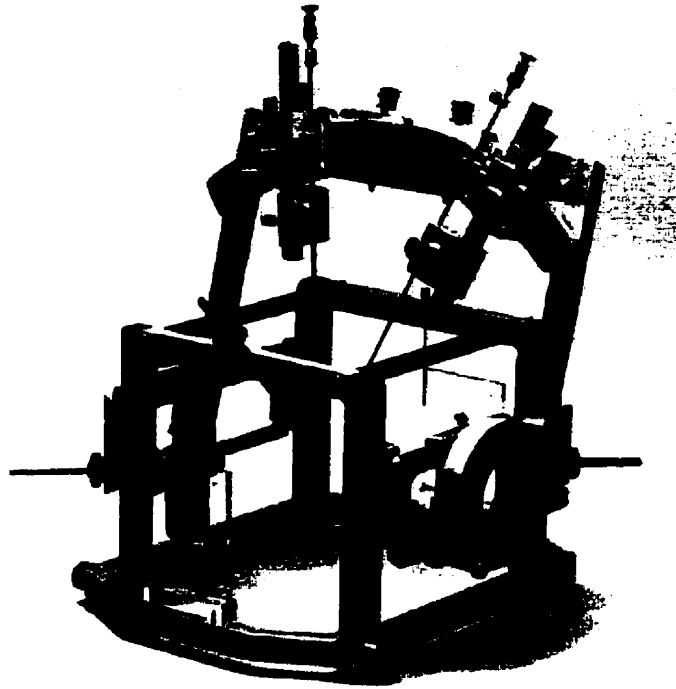


Figure 2.6: The stereotactic frame with the surgical arc system.

2.4.2 Stimulator

The stimulator consists of a rigid hollow metallic shaft with a conducting wire at its centre and an electrode at its tip (see Fig. 2.7). The electrode can be made to protrude from the tip of the probe, in a slightly off-axis fashion, by a specific distance varying from 0 to 14 mm. The tip of the shaft is placed at the target location, and by rotating the shaft, and protruding the electrode with the desired angle and distance, the surgeon can probe the neighborhood of the target. The different areas are stimulated with electrical impulses varying from 0.25 Volt up to 2 Volts. Depending on the patient's reaction, pain, muscle contraction or visual artifact, it is possible to obtain the accurate localization of the electrode and thus precisely determine the site to be lesioned.

2.4.3 Leukotome

The leukotome, shown in Fig. 2.8 is a rigid hollow aluminum shaft with a tiny metallic wire at its centre. The wire can be pushed to protrude from the tip of the shaft to form a "D-shaped" loop.



Figure 2.7: The stimulator.

The tip of the stimulator with the electrode protruding
(8.5:1 magnification).



Figure 2.8: The leukotome.

The tip of the leukotome with the cutting loop open (8.5:1 magnification).

By rotating the shaft by a certain angle, the loop creates a lesion whose shape is a segment of a sphere. The loop extent, varying from 0 to 7 mm, is controlled by the surgeon and the rotation is made in steps of 22.5° , insuring a fairly precise lesioning of the brain.

2.5 Procedure

The surgical procedure begins by first imaging the patient's head with MR one week before the intervention. This preoperative scan is performed with the head coil, resulting in a higher quality image and will serve as the target volume for the atlas registration. Since this volume is available before the operation, the registration does not really have to meet rigid time constraints, and is usually performed the day before. Prior to the intervention, the stereotactic frame is attached to the head under local anesthesia and a burr-hole is drilled on the top of the skull. An MR scan of the patient's head is acquired with the frame on, and an X-ray ventriculogram is made as described earlier. The ventriculogram is used to obtain the accurate localization of certain brain structures, as well as of the target, while the MRI is used to relate the preop scan, along

with the atlas, to the stereotactic system. Once the atlas is superposed onto the patient's brain in frame space, the planning can take place with the help of the ventriculogram. By consulting the segmented MRI of the brain, the shape and location of the volume to excise is specified to follow as closely as possible an "ideal" lesion. After the planning, we proceed with the next stage, which is either performed a few hours after attaching the frame or the next day, depending on time constraints. Using ventriculography and the computed information from the atlas, a stimulation procedure is performed to precisely evaluate the target volume, making sure that only the intended regions will be lesioned. Once this is established, the surgeon proceeds with the target excision using the leukotome.

2.6 Lesion planning

The precise lesioning of the target volume is achieved by carefully selecting the rotation angle and the loop extent. A planning stage is performed using VIPER (see Chapter 5 for more detail) to obtain a lesion that follows as closely as possible an ideal shape. At each level, the loop is opened, rotated and closed to obtain the desired shape. For example, to excise tissue in the shape given by the dark area of Fig. 2.9, the following steps would be performed. First the closed leukotome is aligned to -90° , then the loop is opened to 6 mm. The leukotome is then rotated to -45° where the wire is pulled to 4 mm to reduce the loop size. A rotation to $+45^\circ$ follows and the loop is opened back to 6 mm to be rotated to $+90^\circ$. Finally the loop is retracted to 0 mm. The centre part is completely cut from the outer tissues and will undergo necrosis in the hours following surgery. Fig. 2.9 gives the lateral (or planar) extent of the lesion; the on-axis shape depends on the profile of the loop for the different opening extent. To obtain an adequate lesion volume, this "planar" step is repeated at different levels (or depths). The tip of the leukotome is retracted or pushed deeper in the brain by a few millimeters and a whole new rotation process is performed again. For the particular case of thalamotomies, three levels are usually sufficient to obtain a satisfactory lesion shape.

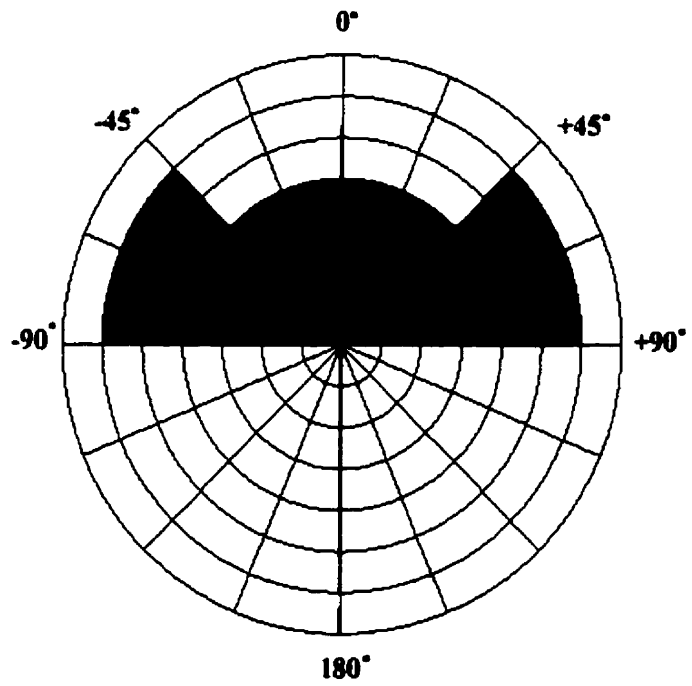


Figure 2.9: The off-axis extent of the lesion.

Chapter 3

Atlas creation

3.1 The atlas data set

We based the construction of our digitized volumetric atlas on the Schaltenbrand and Wahren thalamic atlas [29]. This is the revised version, and although it is fairly old now (it was created in 1977), it is still the most widely used atlas for guidance in the surgical treatment of Parkinson's disease, and was thus the most logical choice for our needs. In this atlas, different brains are cut along either a coronal, sagittal or axial plane, and it should be noted that for a given brain hemisphere, only one of the views is available, i.e. if the hemisphere is cut along the axial plane, coronal and sagittal views of it are not available. We could have built our atlas from any orientation of the sections but since the surgeons rely mostly on the axial sections to extract the information they need (this plane is more or less perpendicular to the trajectory of their surgical tools), we also used this series of slices to build the atlas. The axial sections are done on the right hemisphere of brain number LXXVIII and are displayed in plates 50 to 55 of the atlas. The reference plane orientation is the standard AC-PC plane as defined by Talairach [34]. It is perpendicular to the mid-sagittal plane and passes by the inferior edge of the posterior commissure (PC) and the superior aspect of the anterior commissure (AC). All the other sections are parallel to this reference plane. A mid-sagittal view of the right hemisphere with lines corresponding to the location of the sections is shown in Fig. 3.1. The origin of the atlas coordinate system is

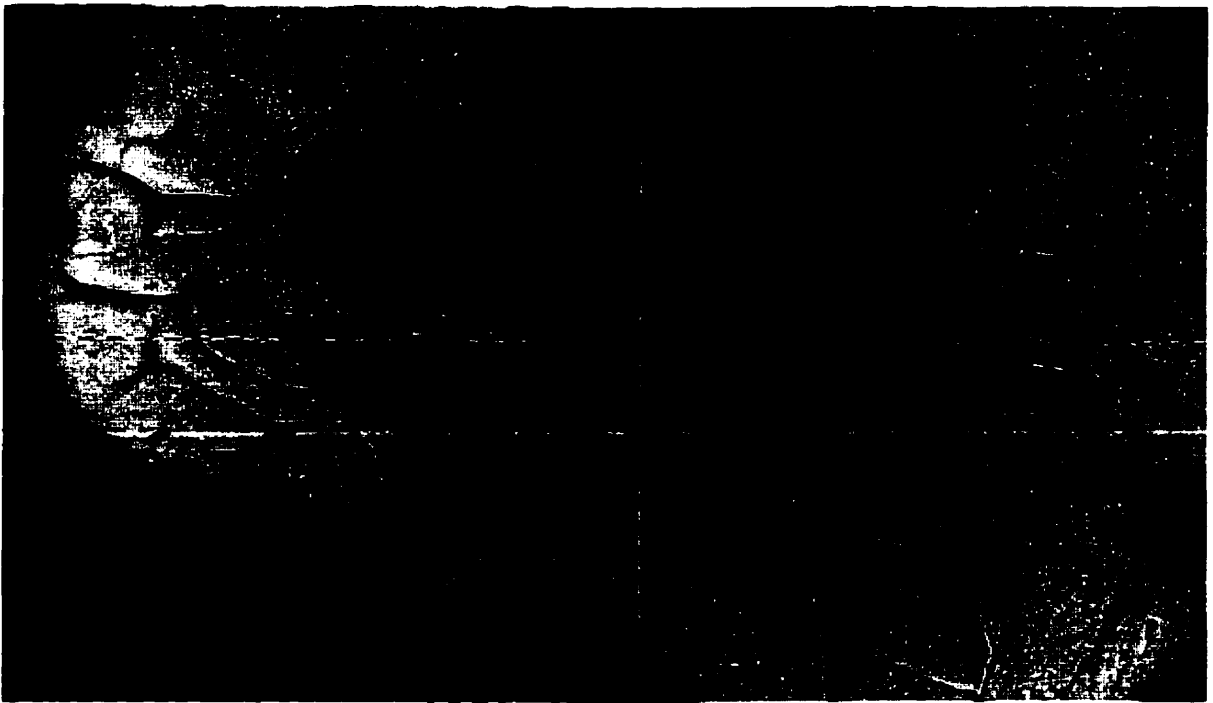


Figure 3.1: Mid sagittal view of the right hemisphere of brain LXXVIII [29] showing axial slices.

situated at the midpoint between the AC and the PC and each section is identified by its distance from the origin, with the positive plane being toward the top of the head.

The atlas itself consists of two parts, the cryotomic photographs and the film overlay. The cryotomic images were obtained by taking pictures of sections of brain placed in paraffin. The pictures were taken with a 4:1 magnification ratio and the brain was myelin stained to give a good anatomical contrast [28]. The cryotome data set comes with a grid to permit the adjacent sections to be aligned as well as for a strict localization within the brain. The spacing of the grid is 1 cm^2 , with one of the lines passing along the mid-sagittal plane. Based on this cryotomic information and on microscopic analysis of the tissues, the regions of the brain were outlined. These contours along with the abbreviation of the region's name are placed on a transparent film that is superposed over the photograph. Fig. 3.2 is an illustration of these two data sets. In the axial series, the sections go from 9 mm below to 16 mm above the AC-PC plane. The spacing between the sections is irregular and varies between 0.5 mm and 3 mm, with the relative finer spacing being concentrated around the AC-PC line. The lateral extent of the atlas is about 4 cm

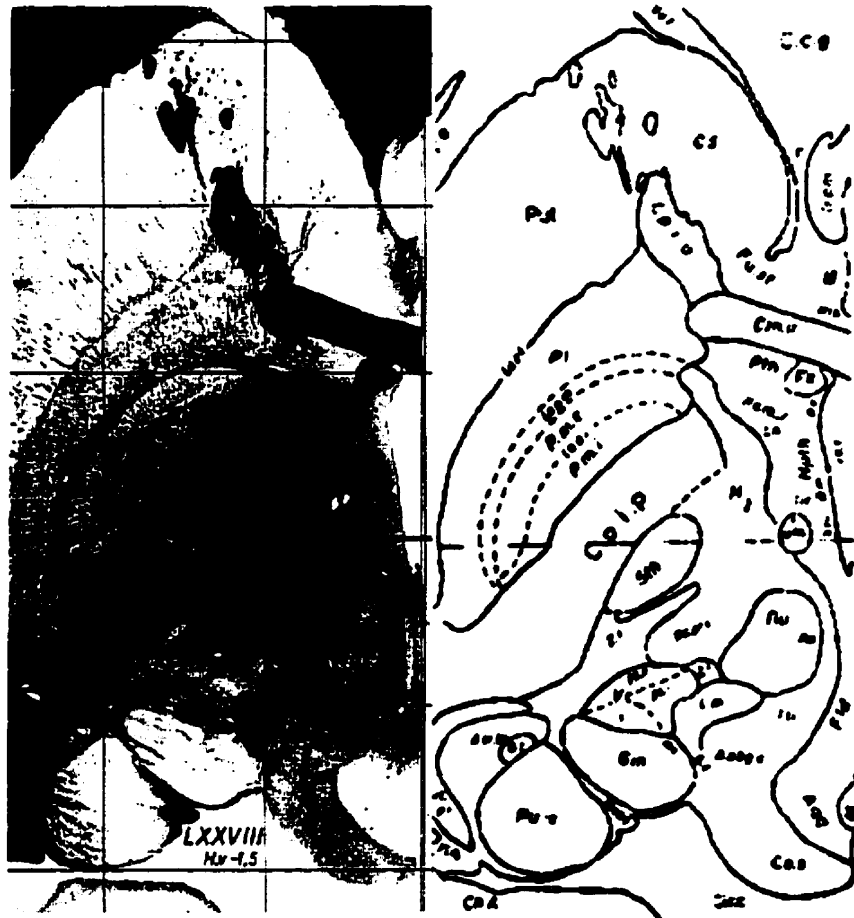


Figure 3.2: The cryotome and film data-sets at the -1.5 mm section [29].

to the left, starting at the mid-sagittal plane, and it covers the region extending from 2 cm anterior to the AC and up to 3 cm posterior to the AC, although some of the sections show only a partial view of that region. The region encompassed by the atlas contains the putamen and thalamus and most of the caudate nucleus.

3.2 The computerized atlas

3.2.1 Digitization

The first step toward obtaining a volumetric version of the atlas was to put all the information it contains in a digitized format. This was performed by scanning the plates of the atlas using a HP ScanJet IIcx flat-bed scanner connected to a personal computer. The cryotome data-set and the film overlay were scanned separately and stored as a bit map (0 or 1) for the film overlay and as a grey scale byte (0 to 255) for the cryosections. Since the film and the cryotomic data sets were binded together it presented some difficulties to scan the film overlay separately, however it was necessary to do so to be able to handle the two data sets independently. Except for one case, the distortion of the image resulting from the scanning (e.g. a scaling or a local stretching of the image) was negligible (see Section 3.3.4). For that special case, because we could not scan the film overlay of section -1.5 mm alone without major distortions, the film information was obtained by extracting the contours from a picture of both the cryotome and film data set scanned together.

With the help of the Photoshop^a picture editing software, we realigned the pictures of the contours with their corresponding cryosections, using rotations and translations. The fitting we obtained was adequate and even better than the original, considering that the initial superposition of the film over the cryosections was not the most accurate. The two pictures, film and cryosection were then linked together, with the same size and same pixel to pixel correspondence.

The scanning resolution was the standard 72 dots per inch (dpi), which was largely sufficient

^a Adobe Photoshop: Adobe System Inc., San Jose, California.

for our needs, and allowed us to work with small (400×700 pixels) pictures. Knowing that the pictures in the atlas are shown with a 4 : 1 magnification ratio, the scanning resolution of 72 dpi yielded a pixel size of 0.0882 mm^2 .

A resolution of a tenth of a millimeter in the brain is more than sufficient for any of our needs and is greater than the inherent accuracy of the atlas.

We then converted these pictures into the MINC format (see Section 2.3). The two dimensional images were converted into a three-dimensional MINC volume. The size of this MINC volume was that of the original picture along the x and y dimensions, with a size of 1 (volume thickness is 1 voxel) along the new z dimension, associated with the position of the sections within the brain. From the MINC files of each section, two large MINC volumes were built, one for the cryotomic data-set and the other for the contour data-set.

3.2.2 Alignment

In order to form a full 3-D volume from these planar volumes, all of the sections needed to be aligned with respect to the others as well as sharing the same sizes. The alignment was done using the grid on the cryotomic pictures. We used as a reference point the intersection of the line 3 cm left of the mid-sagittal line and the line 2 cm posterior to the AC (see Fig. 3.3). All the pictures were aligned with respect to this reference point and were all zero-padded to share the same sizes. This alignment implies that in all the pictures, the reference point would have the same voxel coordinates V_1, V_2, V_3 . Since the contour pictures are linked to their corresponding cryotome images, the two data-sets are also aligned at the same time. Although it corrected only for translations between the pictures, an alignment using only one reference point appeared to be sufficient. No significant rotation between the pictures was visible thanks to a careful positioning of the original pictures during the scanning. However, the superposition of the grid lines between the different pictures at locations other than at the reference point was not perfect. This was caused by distortions resulting from the scanning operation but were not considered to be a significant problem. Particular patterns, such as scaling or major displacement, were not observed and the misalignment of the grid lines between the slices was at most of three vox-



Figure 3.3: The reference point for the alignment.

The selected location for the reference point as indicated by the white arrow.



Figure 3.4: The origin point of the (x, y) axes.

The point selected to represent the origin in the 0.5 mm section as indicated by the black arrow.

els. Considering the pixel (and voxel) size of a tenth of millimeter, this misalignment is judged negligible compared to the inherent accuracy of the atlas (see Section 3.3.4).

Once the pictures were aligned, we had to establish a correspondence between the voxel coordinates and the world coordinates (see Section 2.3 for details on the world to voxel correspondence). By associating the pictures with a world coordinate, we associate to each voxel of the picture its corresponding real location (in mm) within the brain. The x axis was defined as the lateral axis, parallel to the grid lines, with its values increasing from the left to the right. The y axis was defined as parallel to the anterior-posterior grid lines with its values increasing from the back to the front of the head. Both the x and y axes lie in the plane of the sections. For the determination of the x and y world coordinates we forced one point to be the origin. The origin of the (x, y) axes was defined in the picture with an axial value of 0.5 mm as the intersection of the mid-sagittal grid line and the lateral line passing through the AC (see Fig. 3.4). This point (in the +0.5 mm slice) having voxel coordinates of V_{o1}, V_{o2}, V_{o3} would then have world coordinates

(x, y, z) of $0, 0, +0.5$. In all the pictures, the point having voxel coordinate of V_{o1}, V_{o2}, V_3 would then have an (x, y) world coordinate of $(0, 0)$ with a z coordinate equal to its axial value. By setting the origin point we have defined a voxel to world correspondence for every voxel of the picture. It should be noted that since the alignment was performed on another reference point, the voxel having coordinates V_{o1}, V_{o2}, V_3 would not exactly correspond in all the slices to the intersection of the mid-sagittal grid line and the AC lateral line; this is only true for the $+0.5$ mm slice.

The z axis, associated with the height of the section within the brain, runs perpendicular to the plane of the sections. The z coordinate increases from the neck to the top of the head. The size of the voxel in the x and y direction (determined by the scanning resolution) was 0.0882 mm^2 . For the z direction we selected the largest possible size, that is 0.5 mm, considering the minimal separation between the sections. The z space coordinate of each picture was the corresponding axial position of the section (from -9.0 mm to 16.0 mm).

Once all the pictures are assigned their world coordinate, it is possible to build the whole atlas volumes, one for each data-set. To obtain these volumes, the pictures were stacked together, with empty slices at the locations where atlas sections were absent. The result is a volume covering the whole region of the atlas (for the axial series) with each voxel having its world coordinate corresponding to its millimetric location in the atlas. The two volumes, one for each of the cryotome and contour data-set are shown in Fig. 3.5 along the axial, sagittal and coronal views. Any particular point in one volume shares the same world and voxel coordinate as its corresponding point in the other data-set. The volume sizes are $400 \times 634 \times 51$ voxels, the voxel sizes are $0.0882 \times 0.0882 \times 0.5 \text{ mm}^3$ and the ranges run from -34 mm to 1.3 mm, -35 mm to 21 mm and -9.0 mm to 16.0 mm, for the x, y and z directions respectively. The two data-sets were stored in a byte volume with values between 0 and 255 for the cryotome data and with value being either 0 or 255 for the contour data. As we can see in Fig. 3.5, the information can only be retrieved from the axial view of the volume, since the spacing between the sections irregularly varies from 0.5 to 3 mm. We therefore need to obtain a three-dimensional (3-D) definition of the regions to be able to have a real volumetric atlas.

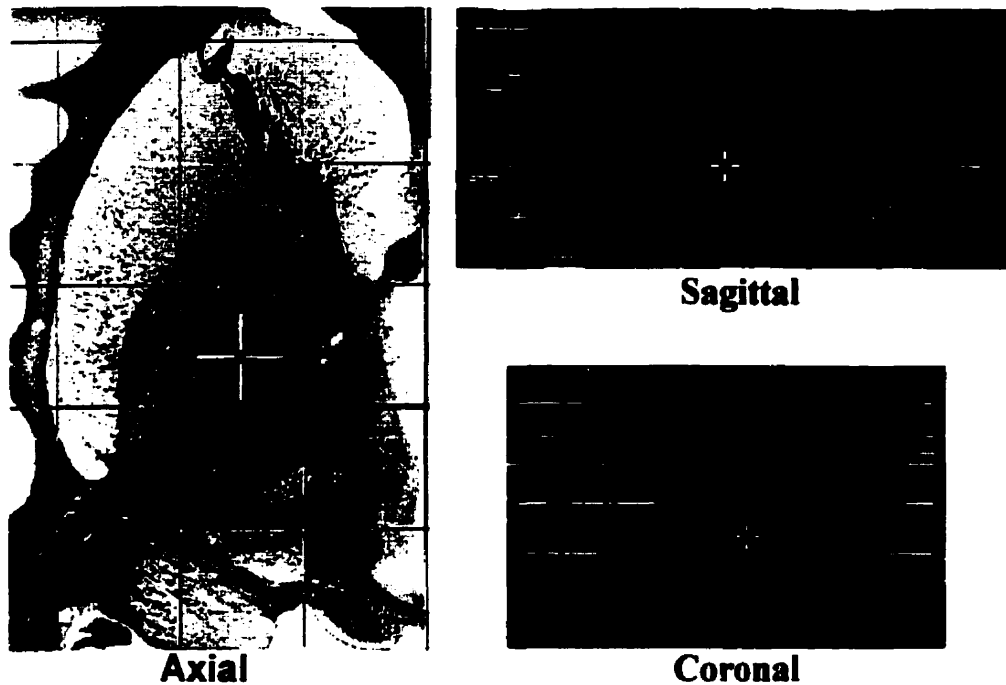


Figure 3.5: The three views of the stacked cryotome volume.

3.3 The three-dimensional atlas

The contour data-set volume served as the basis for the interpolation needed to obtain the required volumetric definition of the regions. The procedure was performed for one region at a time, and was repeated successively for all the regions to be included in the atlas. To be able to perform the interpolation, the contours were first transformed from voxel values (0 or 255) into a vector format, i.e. a list of points, as defined by their three coordinates. The extraction of the points from the contours was performed automatically using a program we created especially for this task.

3.3.1 The vector format

Since closed loops were required to be able to perform the point extraction, some editing on the contour data was needed. Using a painting tool, all the lines or text that interfered with the contour definition were erased, interrupted lines were filled to be continuous and the few noise im-

perfections resulting from the scanning were removed. A more difficult situation appeared when the contours were not complete because the atlas section did not cover the whole region. This was the case for the putamen and caudate nucleus where some of the sections were of restricted size (for instance section 0.5 and -0.5 mm) and for the internal capsule where a definition in a strict fashion is not provided by the atlas. For the putamen and the caudate nucleus, the contours on the sections with a partial view were completed by hand using the next inferior and superior section as a guide, where a complete outline of the region is provided. Although this could in theory lead to quite an arbitrary definition of the region, in the present case the inferior and superior slices gave us very little latitude in the drawing process, leaving almost no place for personal interpretation. In the case of the internal capsule no boundaries were present near the edges of the sections nor at the bottom of the putamen. The definition of these boundaries was decided arbitrarily, with the idea of facilitating the interpolation. However this does not constitute a serious problem for our surgical considerations since in the area where the internal capsule is of interest, its boundaries are well defined by the atlas. It should be also noted that the limit between the putamen, the internal capsule and the caudate nucleus was redrawn in some slices for a better smoothness of the contours.

For the point extraction to be performed, the software needs a starting point located inside the region and a searching direction to be specified. From this point, having voxel value 0, it starts searching voxel-by-voxel, along the specified direction, for a voxel with value 255 corresponding to a point on the curve. From this point, the first of the list, the next point situated at the edge of the curve (point belonging to the curve, having value 255, that is the closest to the body of the region, having value 0) was extracted and added to the list. This was performed sequentially until the whole loop is completed and we return to the first point of the list (see Fig. 3.6). By convention, the curve was always followed in the clockwise direction. For a given region we need all the contours in the different sections to be characterized with the same number of points. From the initial list of points, a fixed number of points (Δ), equally spaced to cover the whole curve, were extracted. For example, for a small region like the internal globus pallidus only 30 points ($\Delta = 30$) were sufficient whereas for a large region like putamen as far as 100 points were extracted. To obtain a good interpolation, the starting point for each curve should



Figure 3.6: Transformation into vector format.

The points extracted of the putamen contour, with $\Delta = 20$ for the illustration purposes.

correspond to similar location of the region at the different sections.

3.3.2 Interpolation

Once the contours are defined in a vector format, the interpolation can be performed. From the contour points, a series of interpolation curves, passing by the contours at the different levels is obtained. For instance the j^{th} interpolation curve is that which passes by all the j^{th} points of the contours at the different sections (see Fig. 3.7). The interpolation curves are calculated using Hermite cubic polynomials (a set of spline parametrization 3-D curves) [12], which assure a continuity of the first order derivative of the curve.

A definition of the contours between the existing sections (i.e. at any given x, y plane) is given by the list of Δ points resulting from the intersection between the Δ interpolation curves and the given x, y plane. To obtain a volumetric definition of the region with a resolution α along the z axis we only need to extract the contour points at all the planes separated by a distance α .

Volume resolution, thus volume size, is a limiting factor in the utilization of visualization software, increasing the time required to load the volume and limiting the real-time interaction with the display windows. For all these reasons we tried to keep the volume sizes as small as possible without losing important information due to a lack of resolution. In the special case of our atlas, since it will be deformed and resampled along any particular plane, for best results it should have an isotropic resolution. The initial planar (x, y) resolution of 0.0882 mm cannot be afforded along the three directions and we actually opted for a 0.25 mm resolution. Considering the extent of the atlas, it results in a fairly small volume ($142 \times 225 \times 103$ voxels). This resolution is nevertheless sufficient considering the accuracy involved with the inherent atlas consistency, the tagging onto the model brain and the process of registering the atlas onto the patient's brain, where a precision of at best 1 mm can be reached.

Now that we have a contour definition in the vector format for all the wanted intermediate sections, we need to reconvert it back to the original voxel format. In each plane, a curve that passes through all the points of the list is obtained by performing an interpolation using, as be-

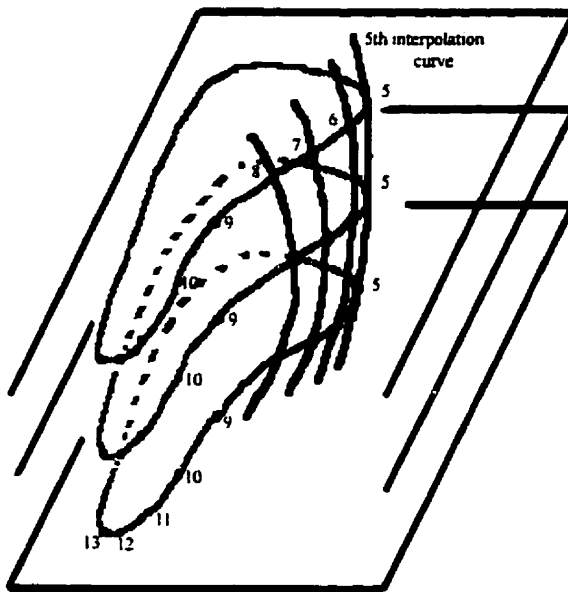


Figure 3.7: The interpolation from the vector contours.

The region's contour at three different levels with the interpolation curves for the 5th, 6th, 7th and 8th points of the vector list.

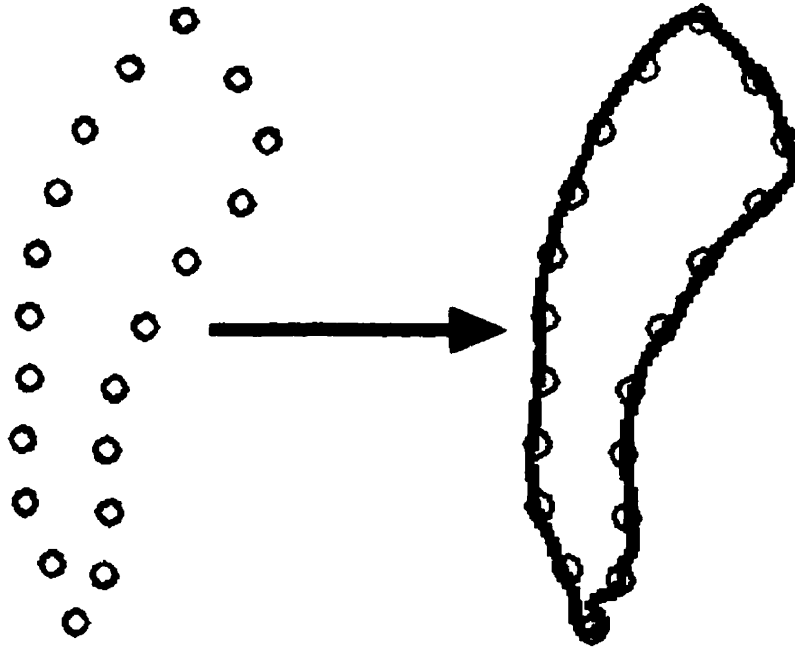


Figure 3.8: From vector format to voxel format.

The return from vector format to voxel format using an interpolation curve.

fore, Hermite polynomials (see Fig. 3.8). From an initial (zero-valued) volume, all the voxels that intersect the interpolation curve had their values changed to 255. This places the contour back into its original voxel format. In order to ensure that our volumetric atlas would have an isotropic resolution of 0.25 mm, the contour points were extracted on planes at every quarter millimeter. The volume used for the conversion from vector format to voxel format also had an isotropic resolution of 0.25 mm.

3.3.3 Image format

Instead of the original 2-D contours, we now have a three dimensional surface giving a real volumetric definition of each region. This format is however not ideally suited for our needs, since surfaces in a voxel format are not particularly easy to work with when a volume deformation is performed (as required for the registration onto the patient's brain), and they do not always repre-

sent the best means of displaying the information during the surgery. We therefore obtained the region's definition as a solid volume, and as a 3-D object to be viewed with a surface-rendering tool. For the solid volume, all the voxels belonging to the region (inside the delimiting surface) are set to a unique value κ , from 1 to 254, for each region. The delimiting voxels could as desired, either keep their initial 255 value to stay as a contour, be changed to the region's value to be assimilated to the region's body, or be changed to 0. We opted for the latter solution in our current atlas since it leaves a small void between the regions, giving a more pleasing appearance to the atlas. We also extracted 3-D objects from these solid volumes using the "Display" software [23]. The 3-D objects are standard files used at the MNI to be displayed with a surface-rendering tool. These surfaces can be translated, rotated and magnified in real time and it provides the best way to get a general notion of the morphology of the region. Different objects (i.e. many regions) can be seen at the same time, allowing the relative positions of the regions to be appreciated. For the special case of surgical guidance we essentially use the solid version, to be superposed onto the patient's brain, and the 3-D objects as an insight for the estimation of the volume to excise.

3.3.4 Drawbacks

Although we have a volumetric definition of the regions, even this is still not ideal. Because the regions are reconstructed from two dimensional sections of the brain, with atlas limitations in terms of spacing between the slices and the overall precision of the definition of the atlas components, the result is not optimum representation of the various thalamic regions. While these limitations are not apparent when the atlas is used in its normal 2-D manner, they lead to the appearance of disturbing features in the 3-D version. As we can see in Fig. 3.9, when a region is viewed along other than the original axial plane (here seen in a coronal view) the edges of the regions appear to be jagged. This behaviour is believed to be caused by inconsistencies between the original sections of the atlas [26]. The source of this problem can be attributed to errors in the accuracy of the positioning of the grid from one slice to the other. In addition, the precision of the drawing of the contour over the boundaries of the regions also plays a role in these errors. If only a misalignment of the grid over the cryosection photograph was involved, we could have

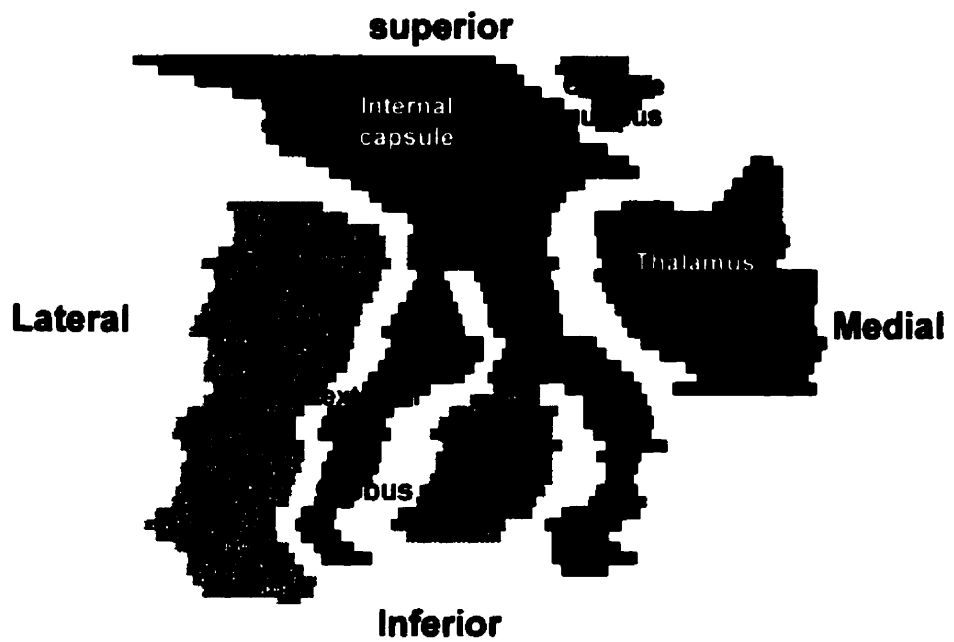


Figure 3.9: Coronal view of the atlas.

A view of the different regions of the volumetric atlas when displayed along a coronal plane.

performed a manual translation on the slices to correct for it. Unfortunately translations alone were not adequate to really improve the quality of the definitions.

This situation should however not be regarded as an overwhelming problem. We may put these limitations in perspective by looking at the context in which the atlas is intended to be used. The atlas should serve as a guidance tool for stereotactic surgery with a desired localization accuracy of around ± 2 mm. This is actually what can be obtained by registering the atlas onto the patient's brain (1–2 mm accuracy). Under these circumstances, the relative imprecision in the definition of the region's edges, being at most of 1 mm, should not be regarded as clinically significant. However, for esthetic reasons (i.e. since we know that the regions do not have jagged boundaries, the 3-D volume and non-axial slices should reflect this), we might want to obtain a smoother outlining of the region. To do so, the region in its solid volume bit map version with value κ for the region's body and 0 outside, is blurred and clamped to share the original voxel value of 0 or κ . The volume is first convoluted with a 3-D Gaussian blurring kernel to smooth its edges. The size of the kernel depends on the level of smoothing expected but a 1 mm FWHM kernel appears to give good results. The volume is then clamped to its original values by forcing all the voxels with a value below and above some threshold to have values of 0 and κ respectively. The threshold should be chosen judiciously for the region's edges to be in the same location as initially (i.e. the region should not be larger or smaller). Although the regions would appear more pleasing after this process, we did not judge this step to be absolutely necessary, therefore we constructed our atlas from the non-smoothed definition of the regions. However this technique might be used in a future, more refined, version of the atlas.

Another problem we faced was the closing of the surface at the top and bottom of the region. The last section, inferior or superior, where the region is defined is not necessarily the inferior or superior end of that region. This is a particular problem when the gap between that section and the next one is as much as 3 mm, and there is a large uncertainty about how and where that region ends. Although they come from other brains, we could have used the sagittal and coronal series of the atlas as a guidance to manually define the extremities of the regions. However, one of our concerns was for the atlas to follow as closely as possible the regions' definitions on the original

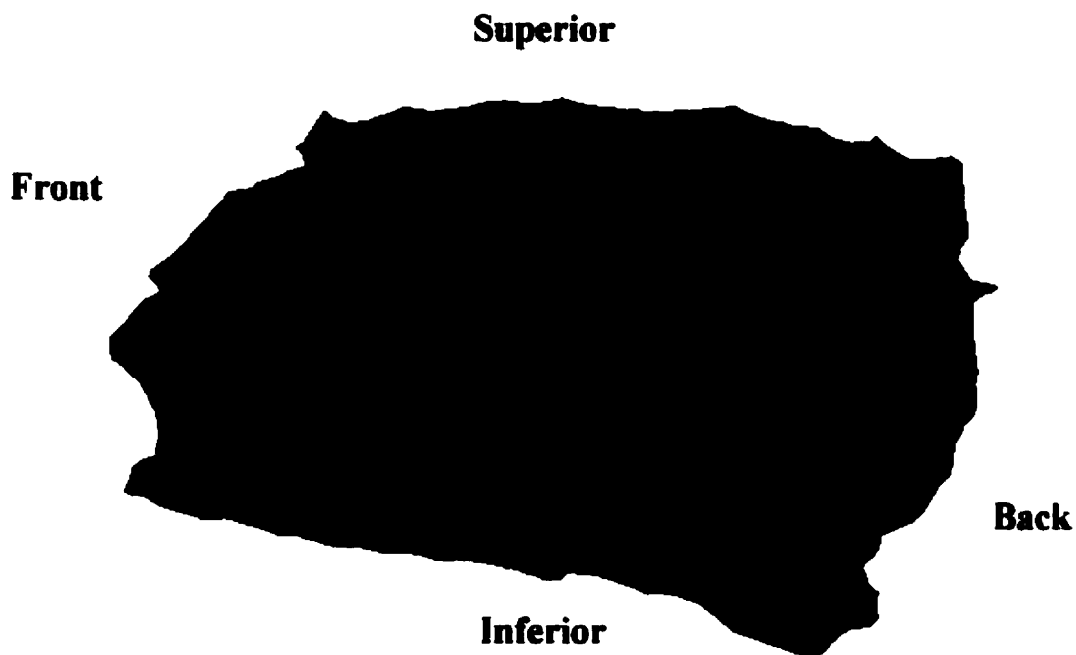


Figure 3.10: Left 3-D view of the putamen.

sections. We therefore tried to keep all contributions from external sources to a minimum. In that sense, we judged that no manual modifications were necessary, and the region's body was closed abruptly at the last section where it was defined; showing as a flat surface at the inferior and superior end of the region. For most of the regions, the area of the region at the extremity sections was much smaller than at its centre; i.e. these extremity sections are situated near the end of the region. This truncated definition is therefore very close to the real region's shape. In some cases however, like the superior end of the putamen, the cut is more drastic (see Fig. 3.10). But since this area is not situated around the lesioning locations, the missing information is not crucial for our surgical guidance needs and we judged this kind of defect as acceptable.

3.3.5 Atlas content

The original atlas includes a huge number of details regarding the definition of the regions and sub-regions. Since it was not necessary to include all this information in our volumetric atlas,

we therefore had to make a selection of the regions it would contain. The goal was to keep a small number of regions, in order not to overload the atlas, and to easily identify them when the atlas would be superposed onto the patient's brain. Structures that are easily recognizable on a MR scan, such as the putamen and anterior commissure, are very useful to verify the accuracy of our registration process and should therefore be included. The rest of the regions we kept were of direct use in the localization and estimation of the volume of the lesion. Some regions are divided into sub-regions. We did not judge pertinent to include such divisions since these details would bring more confusion than information during the surgery.

Following is a list of the selected regions that are defined in our volumetric atlas. For some regions, the decision to include certain structures as part of the region was made by the neurosurgeon directly involved with using the atlas during the surgical procedure. The atlas includes the two large regions of the putamen and the caudate nucleus as well as the anterior commissure; these structures are very easily identifiable on the MR scan. It also contains the main structures of interest, the internal and external globus pallidus, the thalamus and the sub-thalamic nucleus along with two structures that must be spared during the lesioning, the internal capsule and the optic track. In addition to these main structures we added the definition of the principal thalamic nuclei involved with the procedure. These include the ventro intermedialis motor (Vim) nucleus, the internal and external ventro central (Vci, Vce) nuclei, the pulvilinear nucleus, the pf nucleus and the ventro caudal nucleus. This constitutes the most important regions to include in an atlas destined to serve as a guiding tool in the surgical treatment of the Parkinson's disease.

For each of the selected regions, a volumetric definition was obtained in a 3-D object and solid volume version. While for the 3-D surface rendering tool, separate 3-D objects can be viewed together, for the solid volume version, a volume containing all the individual regions needed to be created. With every region having its own voxel value κ , with a value of 0 outside the region's body, the whole volume was merely created by the voxel by voxel addition of all the individual volumes. After this addition was performed, the following minor modifications were made. Between the original sections, some regions, because of the interpolation, had their contour definitions slightly intersecting with each other (e.g. the anterior commissure and the

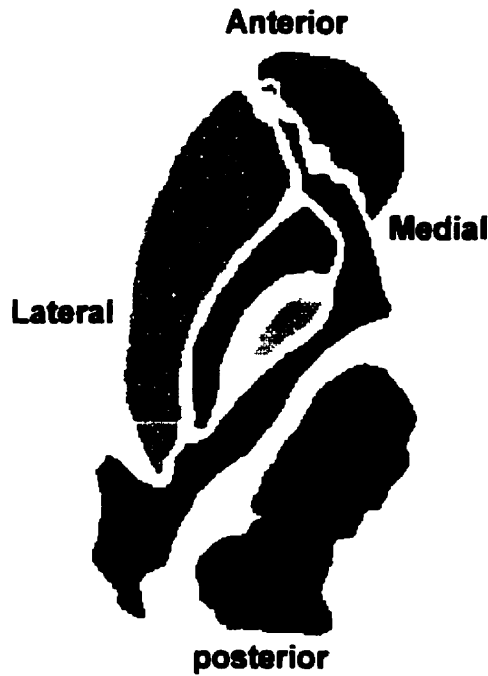


Figure 3.11: An axial view of the atlas.

The structures appearing are the thalamus with the thalamic nuclei, the putamen, the caudate nucleus, the internal and external globus pallidus and the internal capsule.

external globus pallidus). Manual adjustments were performed on the final volume to correct for this effect. For the thalamic nuclei, since they are added in a region already occupied by the thalamus, their values were added to the thalamic value, so the resulting value had to be changed to the initial corresponding thalamic nucleus value. The final atlas volume is shown in Fig. 3.11 in its original view (axial).

The final version of the atlas includes the definition for a special set of selected regions, but any new regions can be easily added to the existing version by simply obtaining its volumetric definition and adding the values to the current atlas.

The atlas volume is defined in an array of bytes and is displayed using a spectral mapping, giving a unique color to the different voxel values. The voxel value attributed to each region was therefore chosen judiciously to assign bright colors to important structures and with the desire to avoid near regions sharing similar colours.

3.4 Segmentation model

We now have available a volumetric definition of the Schaltenbrand and Wahren thalamic atlas [29]. To fully exploit its possibilities as a guiding tool we need to map it to the MRI image of the patient's brain to label the various structures in the patient MRI. To obtain such a mapping, we require the identification of homologous points between the patient and the atlas brains. This step should be performed by a person knowledgeable in neuroanatomy. A good mapping requires the identification of over 100 points requiring a considerable time (more than two hour). One way to circumvent this difficulty is to use the automated image registration tool available at the MNI. This tool, ANIMAL (Automated Nonlinear Image Matching and Anatomical Labeling), described in greater detail in Chapter 4, performs the automatic registration of two MR scans. As an intermediate step the atlas is first mapped to a model MR brain which is subsequently mapped to the patient's brain. By mapping the atlas to a model MR, the time consuming process of identifying homologous points needs to be performed only once, and all the subsequent mapping onto the patient's brain can be achieved automatically by registering the model brain to the patient brain using ANIMAL.

3.4.1 Model MRI

For an optimal atlas-to-patient brain mapping, certain restrictions were imposed in the selection of the model MR brain. For an accurate registration between the two MR scans, the model MR should be acquired using a sequence similar to that used for the patient (the definition of "similar" will be explained in Section 4.1). We also expect the model MR to be of a superior quality in terms of noise and anatomical contrast, for the whole mapping process to suffer the least degradation possible from this intermediate step. The more information it contains, the more accurate will be both the mapping of the atlas onto the model MR and all the future registrations between patient's and model MR. The model we selected is a T_1 -weighted 3-D MR with a 1 mm isotropic resolution, which is the average of 27 scans of the same brain [15]. The acquisition sequence was optimized to give a good grey to white matter contrast. The average of 27 scans resulted in a 3-

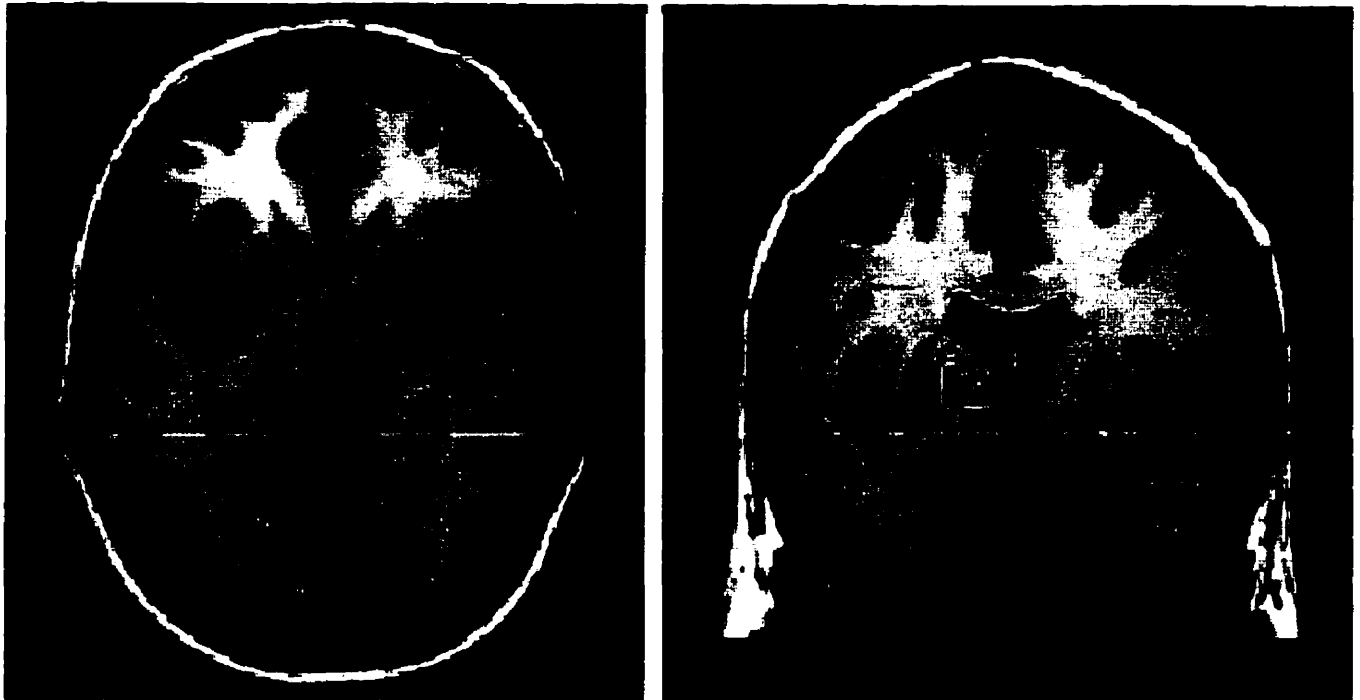


Figure 3.12: The model brain MRI (SuperBrain).

Axial and coronal view of SuperBrain in the thalamic area.

D MR image having a very high signal to noise ratio, which combined with its high resolution, contributes to an MR image showing a lot of anatomical information. A picture of this MR scan (called SuperBrain), viewed along the axial and coronal planes, is shown Fig. 3.12. Such high anatomical detail is very helpful in the identification of the landmarks and thus resulted in a more accurate mapping of the atlas onto the model MR.

3.4.2 Manual tagging

To obtain the warping of the volumetric version of the atlas onto the model MR, we had to identify homologous points in the two brains. By specifying a location (point) in the atlas and by finding its corresponding location in the SuperBrain, we obtained a series of pairs of points from which the deformation needed to map the atlas onto the model MR could be defined. We used a non-linear transformation (thin plate spline) to perform this mapping (see Section 3.4.3). A thorough examination of the SuperBrain, of the cryosections and of the mid-sagittal picture of

the left hemisphere of the atlas's brain led us to the conclusion that the atlas sections and the axial slices of the SuperBrain were coplanar (the standard Talairach orientation). If it had not been the the case, we would have needed to resample the model MR along axes corresponding to those of the original atlas. This is essential for an adequate tagging to be performed, where for every section we need first to find its corresponding plane in the MR. To improve the accuracy of the section-to-slice correspondence between the two brains, the SuperBrain was resampled at a finer resolution along the z axis (axis perpendicular to the section's plane). Using a trilinear interpolation method, the sampling along the z axis was increased from the initial 1 mm to 0.25 mm. Although it does not introduce new information, it allows for a more precise selection of the corresponding plane: with the original sampling of 1mm two sections separated by 0.5 mm in the atlas would have been mapped in the SuperBrain to either the same plane or to two planes separated by 1 mm.

The work of identifying the landmarks was accomplished by Dr. Noor Kabani, an experienced neuroanatomist knowledgeable in the recognition of brain structures on MRI. It was achieved by navigating through the cryotomic data set volume and the SuperBrain volume with a visualization software tool designed for the manual tagging of homologous points in two brains. The first step is to find for every cryosection, its corresponding plane in the model MR. By analyzing the structures, their shape and their location, the neuroanatomist found the plane in the model MR that corresponded the most to the cryosection image. Because of the lack of information relating to thalamic structures on the MRI and also because there are slight anatomical differences between the two brains, the identification of the corresponding plane can vary from one person to another and can also lead to some inconsistencies; e.g. two close sections being matched to two largely separated planes. Such a cryosection-to-MR mapping was performed on four occasions by three different persons and we noticed that the inter-observer variation is limited to about 1 mm, with no mapping inconsistency. These results are encouraging and reinforce the belief that we obtained an adequate localization of the sections onto the model MR. Once this step was accomplished, the neuroanatomist tried to extract the largest number of homologous points for every cryosection.

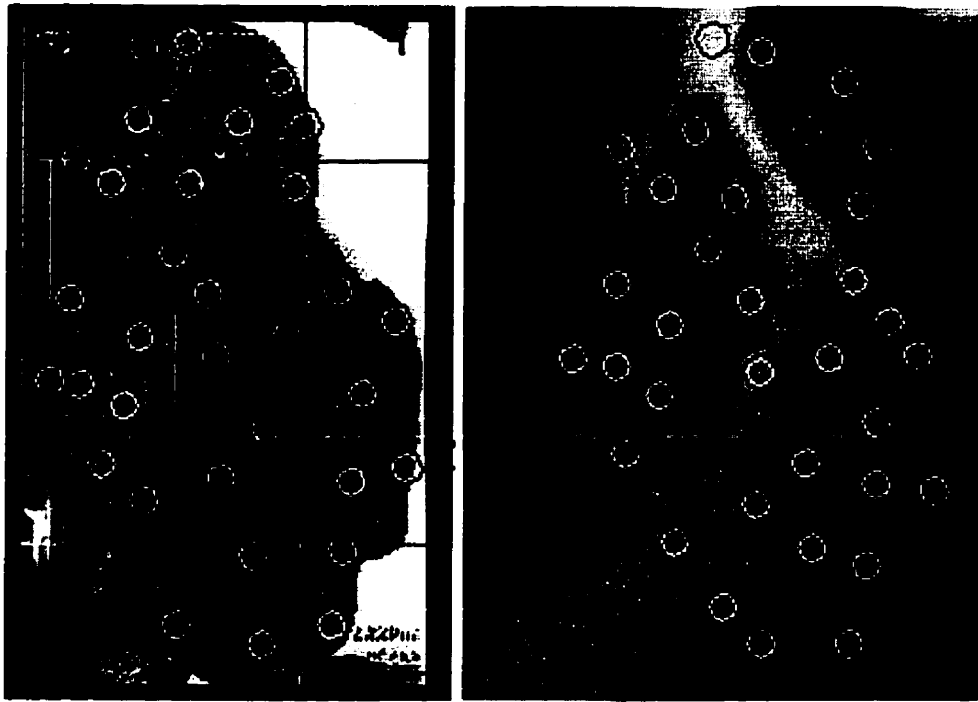


Figure 3.13: The tagging points for the -1.5 mm section.

The tagging points in the -1.5 mm cryotome section and their corresponding location in the model MRI.

The anatomical details on the MR images are limited, and this restricts the number of landmarks that could be recognized in both brains. These points are situated mostly where a good grey-to-white matter contrast is available, like the front tip of the putamen or the intersection of the lateral ventricle and the grey-white matter interface of the caudate nucleus. Because small structures in the white matter appear completely blurred on the MRI, the tagging is carried out essentially on the large grey matter structures, the anterior commissure and the ventricle-white matter interface. It should be noted that structures showing a lot of anatomical variability, like the fornix, do not represent reliable landmarks and were not used in the identification of homologous points. A picture of the tagging points for the section -1.5 mm is shown on Fig. 3.13. As we can see, for grey matter structures the tagging is easily obtained, on the other hand, the identification of the different thalamic nuclei is very difficult. But even without homologous points being identified for these regions, by properly mapping the surrounding structures, the adequate mapping of the thalamic nuclei is also ensured. The final result is a set of 250 pairs of points,

where every cryosection has been tagged, resulting in what we believe is an accurate warping of the atlas onto the model MR brain.

3.4.3 Transformation

The tag points identified above allow a transformation to be computed that warps the atlas onto the MR. The type of transformation we selected for this purpose, the thin plate spline, appeared to be effective for the non-linear mapping of two data-sets together [6, 10, 11]. This is a non-linear transformation where every tag point from the atlas is sent to its corresponding point in the SuperBrain, i.e. the location of a tag point in the atlas is exactly mapped to the location of its homologous point in the SuperBrain. The space in between the tag points is mapped smoothly around its neighboring tag points.

This process ensures that every structure for which a good number of tag points were identified, like the putamen, will have its boundaries fit almost perfectly between the two brains. Regions where only a few or even no points were identified will also benefit from this type of transformation as the stretching imposed by the surrounding structures will induce a deformation meeting specific needs of that local area, i.e. this region will be mapped with respect to its surrounding, instead of following the constraints imposed by the whole atlas volume. The resulting mapping of the atlas onto the model MR is fairly good. Such an accuracy in the mapping could not be achieved by using a linear or even a piecewise-linear transformation.

Even though we used a thin plate spline transformation to obtain the best possible warping, the result could still demonstrate some weakness in terms of mapping accuracy, largely caused by the anatomical differences between the two brains. Although the location and relative size of the deep-seated structures of interest to us is fairly similar from one brain to another, no two brains are exactly the same. Most of the discrepancy in the mapping is caused by the section-to-slice procedure. In this step we try to find the plane on the MR that is the most similar overall to the cryosection image, but not necessarily having the best match for all the individual structures. By looking at the putamen for example, a certain plane might appear to correspond the most, while by looking at another structure, like the caudate nucleus, another plane would perhaps be

more appropriate. The selected plane is thus a trade off between the different structures and does certainly not represent an exact correspondence. The result is a transformation that performs the best warping achievable but that still has some recognised limitations. By closely inspecting the superposition of our warped atlas onto the model MR and by comparing the position of the regions' edges in the two volumes, we believe we have reached a mapping accuracy of around 1–2 mm. We judge this to be sufficient and it certainly corresponds to our need of an overall registration accuracy of the order of 2 mm.

Chapter 4

Registration

Our ultimate goal is to map the volumetric version of the Schaltenbrand and Wahren atlas [29] onto the patient's brain in order to segment the basal ganglia and thalamic structures. By mapping the atlas to a model MR scan, this goal is achieved by obtaining the transformation required to warp the model MR (and thus the atlas) onto the patient's MR. The desired segmentation is therefore achieved automatically. This procedure must be performed for every new patient and should therefore be relatively easy to use while still offering an accurate warping of the atlas to the patient's brain. For this purpose, we used ANIMAL^a, a tool developed at the MNI by Dr. Louis Collins, that performs the registration between two MR images in an automated fashion. A description of this tool is given below.

4.1 Introduction

ANIMAL actually performs the registration between two image volumes obtained within the same modality (e.g. CT to CT, MRI to MRI). MRI is the modality of choice in image guided neurosurgery because of its high resolution and good grey/white matter contrast, so we use this tool for MRI to MRI registration. But even if both images are from the same modality, the two

^a Automatic Nonlinear Image Matching and Anatomical Labeling.

image volumes must also be acquired using similar MR acquisition sequences so that the contrast relationships in each image are similar. The information required to perform the mapping is obtained from the edges and the intensity values of the structures within the images. Therefore, for a structure to be correctly mapped to its homologue, they should share a same relative intensities and their edges should be in similar positions in each image. Whether two MR scans are similar or not is decided by comparing both the intensity and the gradient volumes of the two MR images and by taking into account the degree of registration accuracy expected. In our case, the sequence of the model and of the patient were judged sufficiently similar.

ANIMAL calculates the transformation needed to register a source volume onto a target volume. The target volume must have its feature volumes (blurred and gradient data—see Section 4.2.3) extracted prior to the automated registration. Since this step requires some user intervention, it is performed for the model MR (SuperBrain). This procedure must therefore be performed only once and all the subsequent registrations on patients can then be performed automatically. Since the source volume is the patient MR scan and the target is the model MRI, application of the algorithm results in the transformations that will deform the patient's MR onto the model MR. What we actually need is the reverse, that is, to deform the model MR, along with the atlas, onto the patient's MR image to obtain the needed segmentation. This is achieved by simply applying to the atlas the inverse of the transformation yielded by ANIMAL.

The registration is performed using a non-linear transformation. Although more complex than a simple linear transformation, the non-linear approach was necessary, in order to obtain the desired registration accuracy. Because there are always some slight morphological differences between two brains, the structures will not be perfectly superposed even after a linear registration. A study [11] has shown that on average throughout the whole brain, there is a 6–7 mm anatomical variability still present after the linear registration. While this variability is somewhat less in the basal ganglia, the resulting misalignment is still too important to ignore.

One of the main advantages of ANIMAL is that it is fully automated, performing a non-linear registration between two volumes without user intervention. The use of an automated registration method instead of a manually driven method has many benefits. One of the common pro-

cedures to manually obtain a non-linear registration is to use a thin plate spline transformation [6, 10, 11]. This transformation is calculated from a set of homologous points and thus requires a qualified person to identify a series of landmarks in one volume and their homologue in the other volume. This is a very time consuming task, taking over an hour to identify forty pair of points [8], and even more points could be required depending on the registration accuracy expected. This time consuming step makes this manual approach inappropriate for registrations to be performed on a regular basis, as would be the case for us, where a single surgeon can have many patients per month. As described earlier, with our approach, the manual registration needs to occur only once.

Another drawback of this manual method results from the inability to exactly identify a landmark in the brain. For a given landmark, its localization within the brain may vary from one observer to the other by 1–2 mm [8]. Moreover, a same observer will locate a landmark differently in two occasions separated in time. The transformation will thus vary between the observers, and with time; it will therefore be impossible to regain an initial transformation in a later occasion. This is not the case with the automated method where the two same volumes will always result in the same transformation, a feature that might prove to be useful for future analysis of the present surgical data.

The registration process is accomplished in two steps, first a linear transformation is calculated and then a non-linear deformation field is added to handle the remaining anatomical variability. The next two sections describes the different aspects of these two transformations in greater detail.

4.2 Linear transformation

4.2.1 The transformation

To obtain the registration between the two volumes we need first to obtain a global mapping (or correspondence) between them. This is achieved by linearly mapping the source volume onto

the target. The linear transformation used in this algorithm is a 12 parameter affine transformation. As discussed in Section 2.3, the transformation is always a world to world transformation, from source world coordinate to target world coordinate. The affine transformation is the result of 4 sub-transformations applied in sequence. The first is the translation from the centroid of the source volume to the centroid of the target, while the second is a rigid body rotation. The third step is an anisotropic scaling, with one scaling factor for each axis. Finally a shearing transformation is performed to convert orthogonal axes into a non-orthogonal set if necessary. This transformation takes into account the differences between the scanning orientations (translation and rotation) as well as the basic morphological differences (like brain size) to obtain a global fit of the two brains. It serves as the starting point for the non-linear transformation.

4.2.2 The algorithm approach

The transformation is retrieved using a hierarchical multi-scale algorithm, where hierarchical refers to the fact that a transformation obtained at a coarse scale is passed to a smaller scale to be refined, proceeding in this fashion successively until the final transformation is obtained at the finest scale. The notion of scale refers to the size of the objects of interest, i.e. to the inherent resolution of the data. At a large scale, only the information about the large structures is included. For example, by blurring an image, it is not possible to distinguish the small details anymore. This type of algorithm minimizes the risk of the solution falling into local minima of the optimization function's hyper-surface. It also results in a lower computing time, by as much as a factor of 4, as the computing time to optimize the function strongly decreases with the size of the scale [8].

The algorithm uses the cross-correlation between the extracted features of the two volumes as a measure of the mapping accuracy. The correlation is performed on a subset of voxels in the source volume and on their corresponding location, according to the transformation, in the target volume. The spacing between the voxels of the subset is half the size of the scale used at that step thus following the usual Nyquist criterion. The value of the volume at any given position is interpolated tri-linearly from the data provided by the surrounding voxels. Using a

simplex procedure, an optimization is performed on the transformation's parameter to maximize the value of the cross-correlation between the two volumes.

4.2.3 Features

The cross-correlation between the two volumes is not calculated from the original MRI data but from different features extracted from these MR scans. Such features allow us to introduce the notion of scale, i.e. the size of the structures contributing to the correlation. These features are extracted by convoluting the raw image data with a particular operator satisfying the following conditions: the operator should be linear, and invariant to spatial shift and to rotation. This means that the features extracted from an object should remain the same when this object is translated from one location in the volume to another (spatial shift invariance), or when the object is rotated in the volume (rotational invariance). A solution is the convolution with an isotropic 3-D Gaussian blurring kernel $\mathcal{G}(\vec{r})$ where for every location \vec{r} in the source volume:

$$\mathcal{G}(\vec{r}) = \frac{1}{\sqrt{2\pi\sigma}} e^{-1/2(\frac{r}{\sigma})^2}$$

where σ is the variance of the kernel.

The notion of scale is now introduced by the factor σ where the measure of the scale is given by the full width at half maximum (FWHM = 2.36σ) of the blurring kernel. By blurring the raw image data with the Gaussian kernel, the information coming from the small structures (smaller than the FWHM) is lost and only the large structures contribute to the correlation. The blurred image volume is thus used for the estimation of the mapping transformation at the corresponding scale.

However using only the blurred images to estimate the transformation is not sufficient, and some information about the edges of the structure should be extracted. This is done by using differential operators. The edge information at a given scale is obtained by convoluting the raw image $\mathcal{I}(\vec{r})$ with the partial derivative of the Gaussian kernel.

$$\partial_i f(\vec{r}) = \mathcal{I}(\vec{r}) * \partial_i \mathcal{G}(\vec{r})$$

where $i = x, y, z$ and is the scaled partial derivative along the i axis of the raw image.

The partial derivative along a given axis depends on the orientation of the axis and is therefore not a rotationally invariant feature. Instead, the magnitude of the image gradient is taken as the feature of interest.

$$\|\nabla\| = \sqrt{(\partial_x f)^2 + (\partial_y f)^2 + (\partial_z f)^2}$$

The feature extraction, blurred and gradient data, was performed using “mincblur”, a MINC tool developed at the MNI. The features employed here include both the blurred and the gradient magnitude of the raw intensity image. These satisfy the linearity, shift and rotation invariance and they are well behaved in terms of robustness to noise in the image and continuity between the features extracted at the different scales. The blurred and gradient data at a scale of FWHM = 8 mm are shown in Fig. 4.1.

Including the gradient data to extract the transformation appears to be a judicious choice both in terms of time and accuracy. Departure from the optimal values of the transformation induces much greater variations of the correlation value when the gradient data were used, thus speeding up the optimization procedure considerably. Moreover, by using only the blurred data, the resulting transformation was biased when the source and the target volume did not cover the same extent of the head (e.g. part of the neck may or may not be included in the scan). The result also appeared to be more sensitive to intensity variation across the field of view [8]. Using the gradient data makes the algorithm more robust against these problems.

4.2.4 Procedure

There are different methods of performing the convolution of the raw data with the Gaussian kernels. It can be performed directly in the image domain or alternatively it can take place in Fourier space as the multiplication of the Fourier transform (FT) of the raw data and of the FT of the Gaussian kernel. We opted for the latter of the two methods. The intensity image volume is converted in Fourier space using a 3-D FFT (fast Fourier transform) algorithm [27] and is multiplied with the corresponding Fourier transform of the blurring or derivative kernel. The data

are then transferred back to image space using an inverse FFT resulting in the desired blurred and differential volumes. Since the long tail end of the kernel is not truncated during the computation, this way of proceeding avoids the formation of ring artifacts and is also more robust regarding noise [8].

There are several steps involved in the extraction of the desired linear transformation mapping of the source onto the target volume. We need first to establish the approximate transformation, which will then be used as a starting point for the further optimization. This initial transformation is calculated at the first (largest) scale, from the blurred intensity volume, using a principal axis method [2] giving the initial translation and rotation parameters. The transformation is then refined successively at the different scales using the regular optimization method (cross-correlation) until a final version is obtained.

The selection of the different scales needed to obtain the transformation is based on computing time and on considerations about the inherent information of the images. A factor of two is usually applied when passing from one scale to the next. An initial blur of 32 mm appeared to be too coarse, leaving not enough information for an efficient optimization to be performed, and so the initial scale was 16 mm blurring kernel. At this scale only the blurred intensity volume was used, both for the initial estimation using the principal axis method and for the regular optimization. The transformation then passes to the FWHM = 8 mm scale for further refinement using the blurred and the differential data successively. Finally an additional step at FWHM = 8 mm is performed on the gradient magnitude data using a masked version of the volume to remove the high signal coming from the scalp. This step further improved the brain registration. Passing the transformation to the next scale of 4 mm did not bring any improvement because the correlation between the two brains using only a linear transformation is limited by their morphometric differences.

The use of a multi-scale hierarchical approach greatly reduces the computing time while maintaining an excellent registration accuracy. The algorithm to extract the final transformation takes about 45 min on a SGI R4400 150 MHz UNIX station. This automated method compares favorably to other methods [8] without suffering from the drawbacks of manually based regis-

tration, i.e. time consuming, repeatability and intra-observer variability.

4.3 Non-linear transformation

Because two brains always show some morphological differences, a given point in the source brain will not always be mapped to its homologous point in the target brain when using a simple linear transformation. To take into account this anatomical variability it is necessary to employ a transformation that allows for more degrees of freedom than simply the 12 parameters of the linear transform. By using such a non-linear transformation we could theoretically map every point of the source to its homologue in the target brain. However for this transformation to be possible, it is necessary for the two data-sets to be topologically equivalent (i.e. there should exist a one to one correspondence between every point of the two brains). Unfortunately this is not the case at a fine scale for the human brain. As we go to successively finer and finer scales, different structures appear for which a one to one correspondence is not available. For instance at a scale less than $\text{FWHM} = 8 \text{ mm}$, some cortical structures are not topologically equivalent. Fortunately this is not the case for the basal ganglia structures and we can thus expect the atlas to be mapped onto the patient's brain within the 2 mm localization accuracy.

4.3.1 The transformation

The linear transformation obtained by the previous algorithm is taken as the starting point for the estimation of the non-linear deformation field that will accurately register SuperBrain to the patient's MR. The non-linear transformation \mathcal{N} used to warp the source MR onto the target MR is the concatenation of two transformations: the linear transformation \mathcal{L} previously extracted and a non-linear deformation \mathcal{D} to be extracted. For any point \vec{r} in the source volume:

$$\mathcal{N}(\vec{r}) = \mathcal{L}(\vec{r}) + \mathcal{D}(\mathcal{L}(\vec{r}))$$

with as usual \mathcal{N} refers to the world-to-world transformation from source to target. The non-linear component \mathcal{D} of the transformation is given as a deformation field, where for each voxel

of the volume, a displacement vector (translations t_x , t_y and t_z) is specified. This deformation is obtained using a principle similar to that used to extract the linear transform. Instead of searching for a global mapping between the source and the target volume, the mapping is performed locally on a set of small regions of the brain.

For every point of a regularly spaced lattice, a local neighborhood is mapped using only a translation to its corresponding location in the target volume. From the translation (t_x, t_y, t_z) obtained at every lattice point, the deformation field is calculated for every voxel using tri-cubic interpolation. Since this field is a representation of the actual physical deformation of a given brain, it must satisfy some specific constraints (i.e. the amount of stretching or compression of a region with respect to the model, must fall within anatomical limits). This imposes some restrictions on the smoothness of the deformation field. It also limits the region in the target volume where a given local neighborhood in the source brain can be mapped, thus reducing the time needed for the optimization.

4.3.2 The algorithm approach

The non-linear deformation is also extracted in a hierarchical multi-scale fashion where the transformation obtained at one scale is passed to the next step for further refinement.

In order to calculate the deformation field, the displacement vector must be estimated at various points scattered throughout the brain. These points are positioned on a regularly spaced 3-D lattice with a sampling interval equal to half the FWHM at the given scale. For each of these points, the displacement vector is estimated using the cross-correlation between the two volumes as a measure of the registration accuracy. The optimization of the translation parameters is performed using a simplex procedure with a tolerance of 0.01 [8]. Because of anatomical constraints, the displacement must fall within a certain distance from the original position, thus limiting the searching range during the optimization procedure. As for the linear registration, the correlation is performed using the usual scaled features of blurred and gradient magnitude data. Since this displacement is applied to a local region around the point, the cross-correlation is calculated only over a small neighborhood of that point.

The size of the neighborhood was chosen to be equal to $3/2$ FWHM. This choice was a good compromise between a large region area ensuring continuity of the deformation field and a small area allowing the displacement to be more specific to that particular region. Since the inherent resolution of the gradient data is twice that of the blurred data at the same scale, the cross-correlation needs to be performed on the local neighborhood using a sampling rate of $1/4$ FWHM. For example, at a scale of 8 mm FWHM, see Fig. 4.2, the deformation field is estimated for a series of points organized in a 3-D cubic lattice and separated by 4 mm. For each of the lattice points, the displacement vector is optimized using the cross-correlation between a sphere with a 12 mm diameter centered around the lattice point and its corresponding region in the target volume. The correlation is performed on a sub-set of points from this sphere with a spacing between the points equal to 2 mm ($1/4$ FWHM). With a diameter of $3/2$ FWHM, the neighborhood of adjacent lattice points intersects with each other resulting in a good deformation field continuity. It also means that the correlation value at a given node is influenced by the value of the displacement vector of surrounding nodes. Consequently the optimizations of the deformation field at the different nodes are not independent of each other. We therefore had to resort to an iterative procedure for the estimation of the displacement vectors. After each optimization, only a fraction (α) of the calculated additional displacement served to update the deformation field which will be used at the next iteration. It appeared [8] experimentally that a value of α between 0.2 to 0.5 is a good compromise between reducing the number of iterations (speed) and insuring a good field continuity. A smoothing of the displacement vectors is also performed in order for them to realistically represent, a physical deformation of the brain, with its underlying constraints.

4.3.3 Procedure

Here again the scales were selected using a factor of two between them with the finest scale being 4 mm (FWHM). Tests made using a final refinement of the transformation at a 2 mm scale showed that the improvement of registration accuracy was not significant compared to the large increase in computing time [8]. The refinement algorithm was thus stopped at the 4 mm scale.

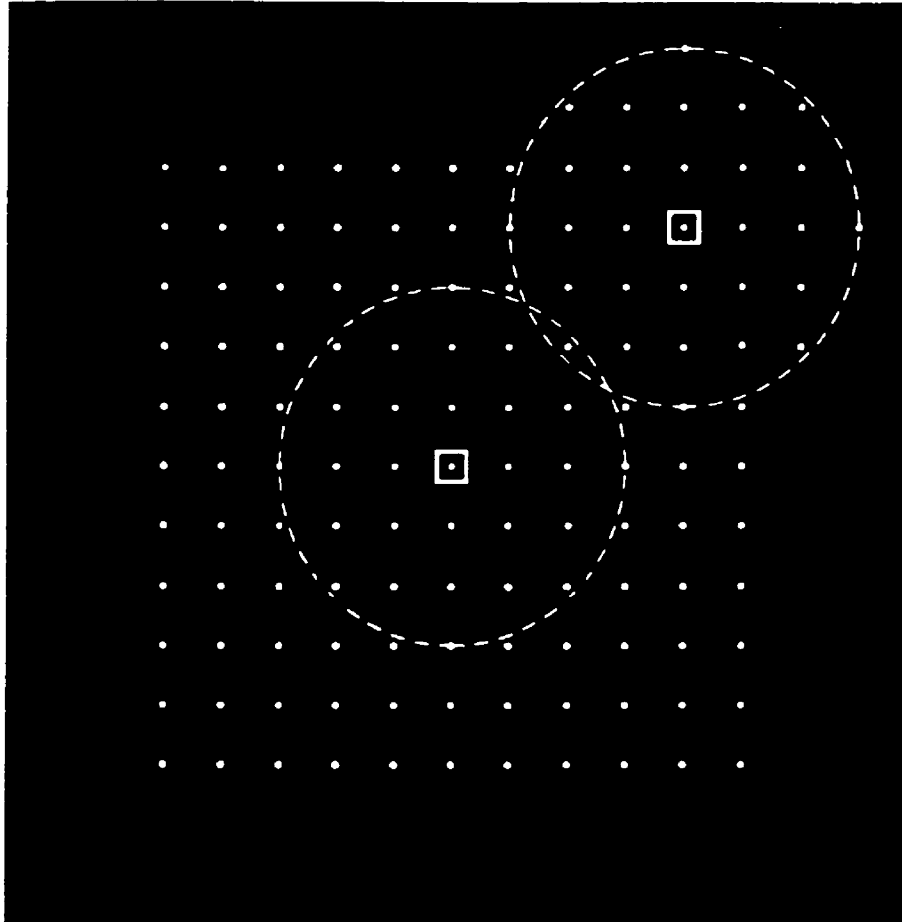


Figure 4.2: The lattice sampling.

The lattice sampling process at the 8 mm FWHM scale on a 1 mm^3 pixel resolution data-set. Squares are at locations where the deformation field is estimated, circles represent the delimiting $3/2$ FWHM neighborhood sphere, white dots that fall inside the sphere are used as sampling points in the computation of the cross-correlation.

At the other limit, because the information about the structures obtained at a scale of 32 mm was insufficient for an efficient optimization to be performed, the initial scale was set to 16 mm (FWHM). However, an extra initial step was added at a scale of 24 mm. In this first step the deformation field was estimated at every point on a 12 mm (1/2 FWHM) lattice, but using the features (blurred and gradient) extracted at a FWHM=16 mm scale. This initial step contributes to reducing the computing time by rapidly obtaining an approximate deformation field which is then passed to the regular 16 mm, 8 mm and 4 mm scale steps for further refinements.

The overall computing time for the estimation of the deformation field is around 6 hours on a SGI R4400 150 MHz unit. This is a fairly large amount of time but we have to keep in mind that it is a fully automated registration method thus not necessitating any user's intervention during the computation. For the special case of interest to us, the registration is performed overnight before the operation; time is therefore not a limiting factor.

The final registration accuracy obtained with this method is comparable [8] to that of a manual warping method (Thin Plate Spline) without necessitating a labor intensive, time consuming step, such as the identification of brain landmarks. This automated procedure is therefore the method of choice for situations where the registration must be performed on a regular basis, as in our case. The result of using this registration tool is the global non-linear transformation (linear transformation plus non-linear deformation field) that maps the source (patient) onto the target (model). The inverse of this transformation then specifies the warp that must be applied to the model MR (SuperBrain) to match it to the target (patient) brain. The volumetric atlas is simultaneously mapped onto the patient's brain, and results in the desired segmentation in the basal ganglia and thalamic structures. After the registration, the anatomical overlap between the two brains in the region of interest to us is of the order 1–2 mm and thus meets our needs of a target accuracy of 2 mm.

Chapter 5

Imaging platform

The imaging platform is a central element of image guided neurosurgery (IGNS). Its role is to provide a means of displaying most of the available information from the patient but also to facilitate the different tasks involved with the surgery. The platform commonly used at the MNI for the different surgical procedures is the Viewing Wand, from ISG Technologies^a. Although it provides the essential features for IGNS, it is important to be able to add new tools to it, especially in a research environment like ours. These additions are relatively hard to perform on this platform, which constitute a serious limitation in the development of an image software satisfying the particular needs of thalamotomy for example. To solve this problem, a new visualization platform was developed here by the IGNS group. The software, called VIPER (Visual Integration Platform for Enhanced Reality) is coded in C++ and uses the two well-known libraries Motif [7] and Open GL [18], therefore making any modification or addition to it a relatively simple task. The main features of VIPER along with the particular tools used in thalamotomy will be described in the next sections.

^a I.S.G. Technologies Inc., Mississauga, Ontario, Canada.

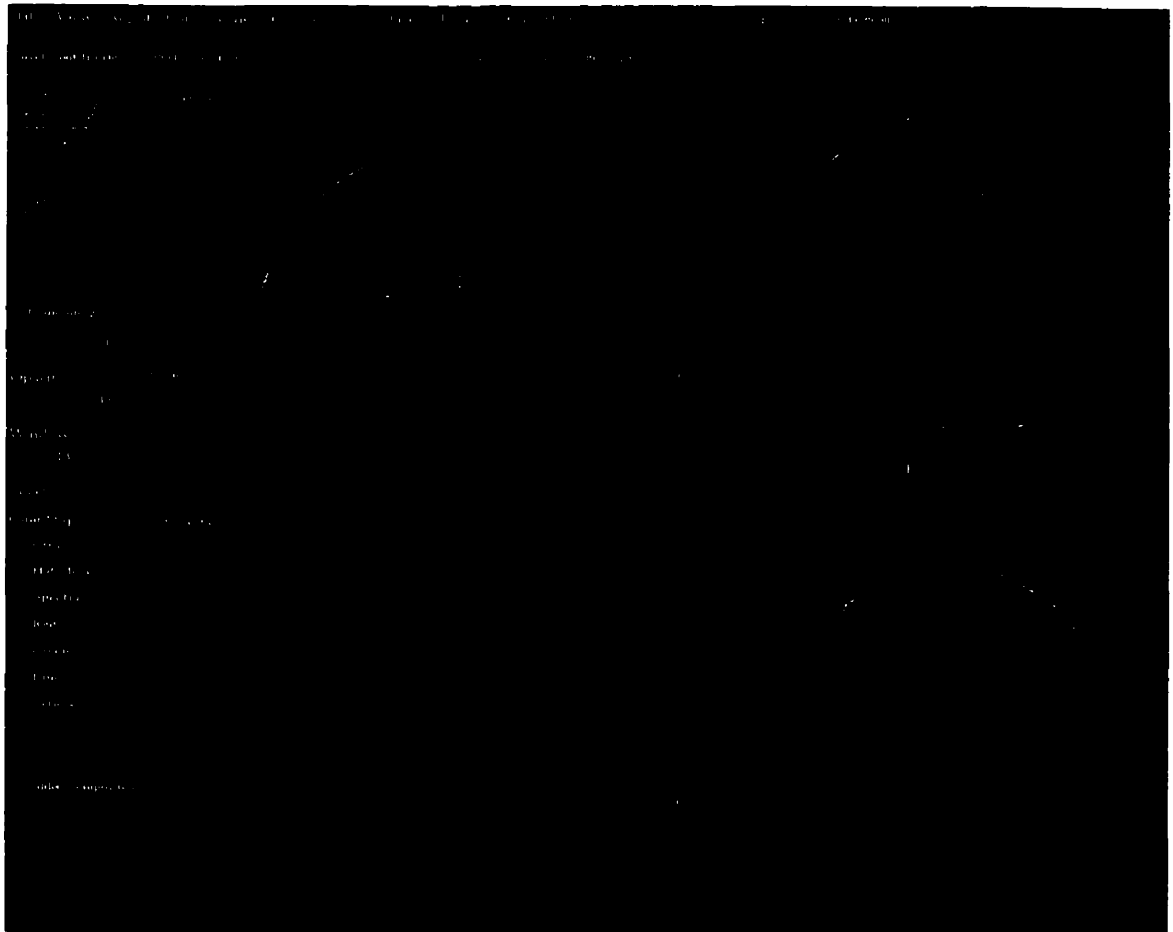


Figure 5.1: The imaging platform

An overall view of the VIPER platform showing the four display windows and the different menu buttons.

5.1 Navigation

In its general aspect, the VIPER platform (shown in Fig. 5.1) consists of four visualization windows for the navigation through the image volume and a series of menu buttons to select the different tools. The windows are used to display 2-D sections of the volume along the three standard orientations, coronal, sagittal and axial. By default, these three views are initially assigned to the first three windows but any of the four windows can independently display any of the standard planes and trajectory view sections as well as 3-D surfaces (the last two options will be discussed in Sections 5.3.1 and 5.2 respectively). The position of these sections inside

the image volume is dictated by the position of the cursor, corresponding to the intersection of the three standard planes. This cursor, at the centre of the cross hairs, can be moved by clicking with the mouse at different locations of the volume in any of the three windows. Alternatively, arrows can be used to move slice by slice across the volume. Zooming and translations are also provided for optimal visualization using simple scroll bars on the side of the windows. One of the most interesting features of VIPER is the possibility to display different image volumes superposed on each other. A primary volume, usually MRI because it provides a good anatomical context for the other modalities, and up to seven secondary volumes can be displayed together, with the superposition made according to their world coordinate system. The volumes can be acquired at different resolution and with different fields of view without affecting their display. For all the secondary volumes, only the data that falls within the field of view of the primary volume will be displayed but they will all appear with their original resolution. This particularity is very important since we need to keep a detailed high resolution (0.25 mm) volumetric atlas when displayed over the patient's MR having a 1 or 1.5 mm resolution. To superpose the different modalities, each volume is displayed with a different color map selected from greyscale, hot metal, blue, red, green and yellow. They are then blended together by selecting for each modality an opacity level, between 0 and 1, giving the relative weight of that modality with respect to the others.

5.2 3-D rendering

Beside the 2-D planar views, volume and surface rendering tools are also available, giving a 3-D view of the volume data. A stereoscopic mode can also be used to obtain optimal information about the tri-dimensionality of the displayed objects.

5.2.1 Volume rendering

Unlike a 2-D section cut inside the volume, a volume-rendering picture contains information about the whole volume. It gives more or less an image similar to an X-ray of the volume with



Figure 5.2: Grey matter weighted volume rendering view of the SuperBrain.

the source being located at the observer's eye. For each ray, the projection result is the weighted sum of the value of all the voxels struck by that virtual ray (by weighted sum we imply that the relative weight of a voxel in the sum will depend on certain factors like its voxel value or its position inside the ray path). The result is a fuzzy image of the volume, as if it was translucent, with a certain feeling of the brain anatomy. A grey matter weighted volume rendering of a brain MR scan is shown in Fig. 5.2. Although a single view gives little anatomical information, by rotating the volume (i.e. changing the viewing orientation), the position of the different structures becomes more apparent.

5.2.2 Surface rendering

Another method for displaying 3-D information is to use surface rendering. In this case, 3-D surfaces need first to be extracted from the volume; they could be for instance, the cortex surface, the grey-to-white matter interface or the boundary of an internal structure such as thalamic

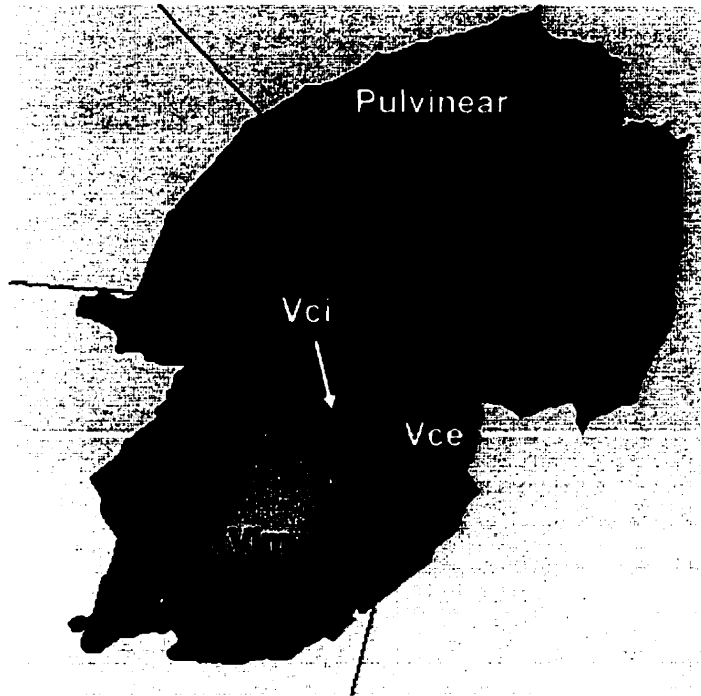


Figure 5.3: A 3-D view of the thalamic nuclei.

The structures included are the pulvinaer, Vci, Vce, Vim and Ce nuclei.

nuclei. The surfaces are then displayed by simulating different lighting and shading effects to give an impression of their 3-D shape. Many 3-D objects (surfaces) can be viewed at the same time in VIPER with each object having a given color and opacity level. Fig. 5.3 shows a view of the various thalamic nuclei. The image can be rotated, zoomed and shifted in real time, to give a good appreciation of the global positioning of the different structures. Six standard views (i.e. front, back, left, right, bottom and top) can also be selected for a rapid reorientation of the objects.

5.2.3 Stereoscopic view

An optimal viewing of these 3-D surfaces can be achieved by viewing them using stereoscopic mode. By alternately sending left and right eye views of the objects in synchronization with stereoscopic glasses, each eye sees its corresponding image.

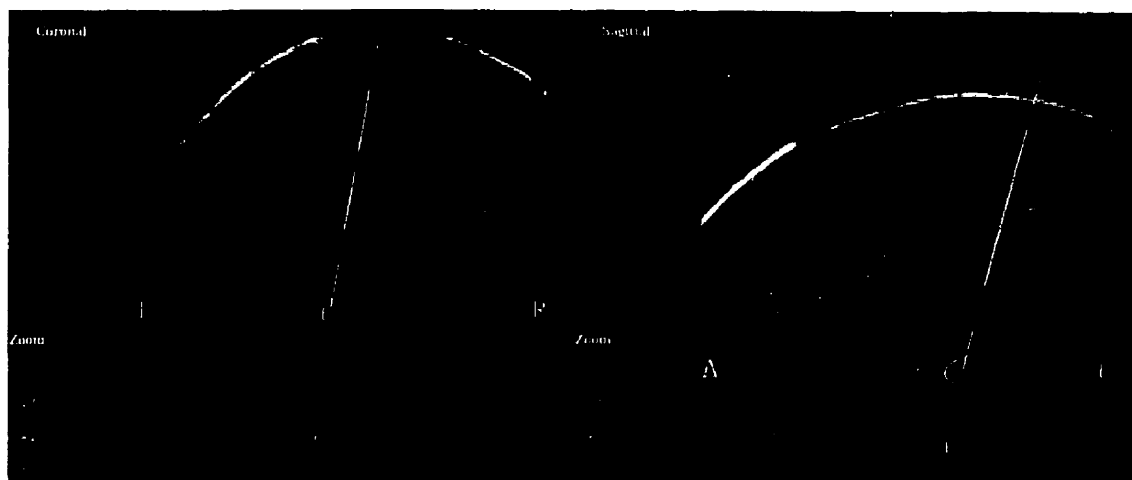


Figure 5.4: The leukotome in the planar views.

2-D sections of the MRI with the leukotome projected onto them.

5.3 Surgery oriented tools

Along with the standard visualization tools of VIPER, special tools particularly useful for thalamotomy were also implemented. They are designed to provide the surgeon with a better guidance as well as making different surgical tasks easier.

5.3.1 Modeling of the surgical tools

The two principal tools used during surgery, namely the leukotome and the stimulator, have been modeled in the VIPER environment in order to simulate their presence in the images. The exact shape of the cutting loop and the position of the protruding electrode have been taken into account at all the different levels of extension. By specifying the position of its tip (target), the insertion angle (declination and azimuth), the loop or electrode extent, and the twist angle (rotation along the shaft axis) it is possible to visualize the tool in the viewing windows. With the 2-D section view, a projection of the tool along the plane instead of an actual section of it is displayed. Fig. 5.4 and Fig. 5.5 show respectively the leukotome in the 2-D section and in the 3-D surface views. Besides the three standard planar views, two trajectory views are also available.

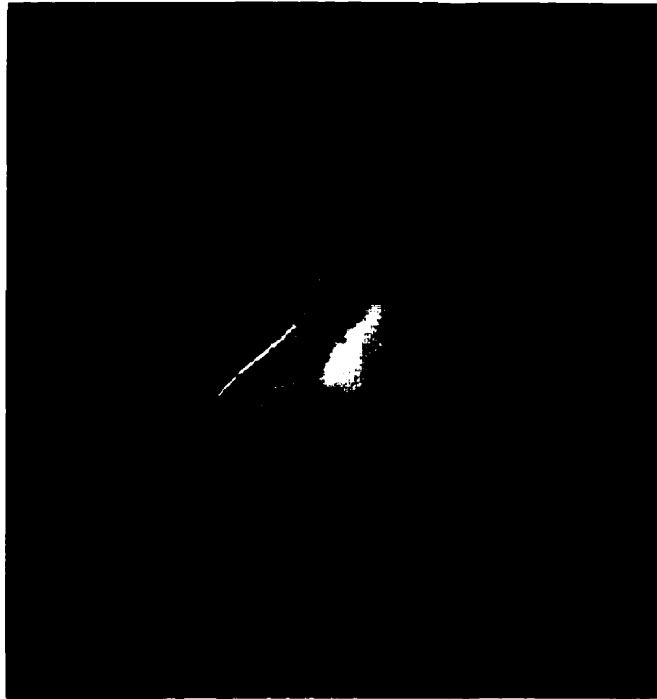


Figure 5.5: The leukotome with 3-D objects.

3-D view of the leukotome in the thalamic area.

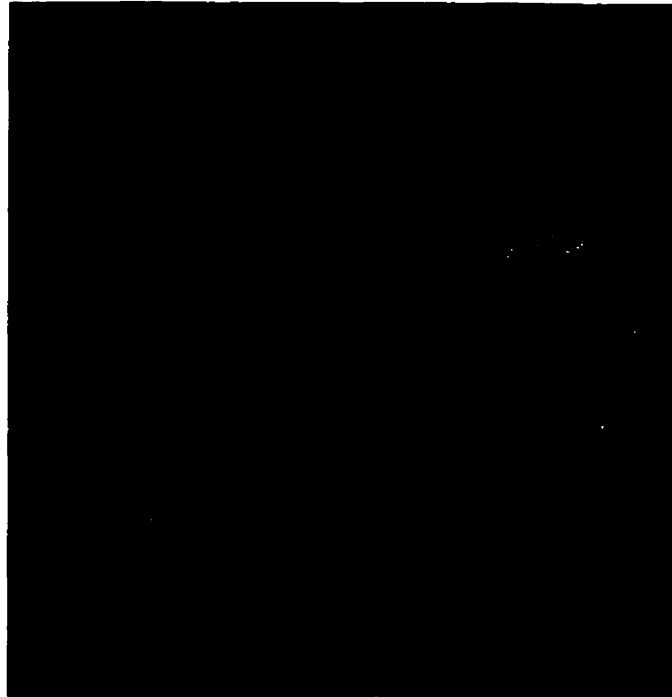


Figure 5.6: The perpendicular trajectory view.

A view of the patient's MRI along a section perpendicular to the axis of the leukotome and passing by its tip.

The first view is the section perpendicular to the shaft axis and passing by its tip while the second is the section along the tool axis and aligned with the twist angle. A perpendicular view, as shown in Fig. 5.6, can be very useful during the planning of the lesion.

5.3.2 Lesion planning

By interactively modifying the loop opening and the twist angle of the leukotome with both the planar views and the 3-D surfaces, the surgeon can estimate what would result in an appropriate lesion of the basal ganglia or thalamus. He then selects a tool that will model the volume of the planned lesion. A window pops up with a target corresponding to the off-axis extent of the lesion (see Fig. 5.7). The target area is divided into sixteen sections corresponding to rotation of the twist angle by 22.5° and seven concentric rings corresponding to the different extents of the loop opening. With a simple mouse click, the areas to be excised are selected. Then, based on

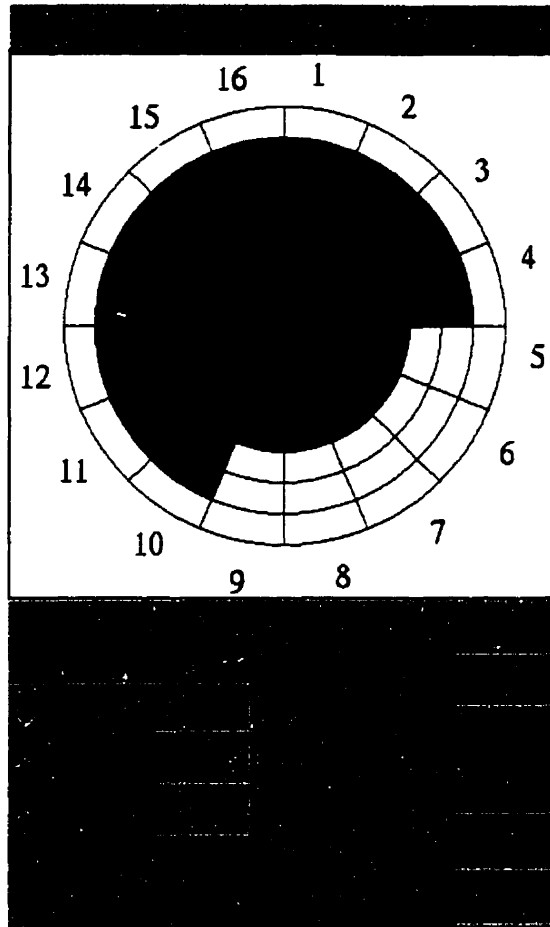


Figure 5.7: The lesion planning tool.

The lesion planning window with the target area divided into 112 sectors and a selection panel for the target location, the trajectory angles and the position of the different levels.

the modeled shape of the loop, the 3-D volume corresponding to this virtual lesion is computed. This step is repeated at different levels (usually three levels in total) corresponding to pulling or pushing the leukotome a few millimeters above or below the centre of the target, in order to obtain better control of the 3-D extent of the lesion. The global virtual excision volume can then be superposed over the other modalities (the MRI and the atlas) in either the planar views or with the 3-D surfaces to verify its adequacy. Modification to the planned lesion can be performed until the resulting volume is sufficiently similar to the desired lesion volume. This gives a more precise lesioning of the selected region, which will hopefully increase the success rate of the operation.

5.3.3 MR to frame space

Another interesting feature of VIPER is the possibility to calculate easily the transformation from the MR space to the stereotactic frame space. Since the frame fiducial markers are apparent on the MR scan, a program was developed to obtain the transformation relating the two spaces by simply clicking, in an ordered fashion, at the location where the markers appear on the 2-D sections window.

5.3.4 Annotations

During the stimulation procedure, certain points of the basal ganglia or thalamus are electrically stimulated while the surgeon monitors the physical reaction produced in the patient. VIPER provides a simple annotation tool that stores the position (coordinate) of the stimulation point and allows a description of the patient's reaction along with the electrical voltage used to be recorded on the screen. This information can then be used in later studies, for instance in the development of a functional atlas of the thalamic region.

Chapter 6

Conclusion and Future Work

6.1 Conclusion

Our initial goal was to provide the surgeon with a better insight of the anatomy of the patient brain. In order to achieve this, the central element was to obtain a mapping of the Schaltenbrand and Wahren thalamic atlas onto the patient's MRI of brain. This was successfully performed by obtaining the volumetric version of the atlas, then by mapping it to a model MRI and finally by registering it to the patient's MRI. The final registration used a non-linear transformation resulting in an accurate labeling of the patient's MRI. This step is performed automatically and is therefore ideally suited for such a procedure, which needs to be performed on a routine basis. Along with the labeling of the patient brain, different visualization and planning tools were also developed to help the surgeon with the different surgical tasks. The idea was to take advantage of the new possibilities allowed by the computer technology and use them in improving the surgical procedure commonly used. The whole system, registration of the atlas along with the visualization platform and its tools, has now been incorporated as an essential element of the surgical procedure. It has already been used for over 10 cases and the surgeon in charge of the operation, Dr. Sadikot, has expressed his satisfaction with it. The system greatly facilitates the surgical procedure both for the planning and the guidance and it will now be used for all the subsequent surgeries associated with the treatment of Parkinson's disease at MNI.

6.2 Future Work

Atlas refinements: Some minor modifications to the atlas might be considered in a future version. For instance, the jagged edge problem resulting from the misalignment of the original sections could be corrected by smoothing the regions' edges, giving a better appearance to the atlas. Also some new regions and or details might be added as the surgeon feels the need for it. Instead of adding these features to the regular atlas version they would be displayed separately and toggled on or off from the screen when required, thus avoiding an overloading of the regular atlas version.

Functional atlas: Based on the stimulation runs performed prior to the lesioning, a probabilistic functional atlas could be developed. An important data set, 50 cases, coming from the surgical procedures performed by Dr. Sadikot, is kept in files. These records include the stimulation position in the frame stereotactic space, the voltage, the corresponding physical response as well as the MRI scans of the patients. The atlas would then be registered to the patient MRI and from a plot of the stimulation points onto the atlas, a probabilistic functional atlas could be extracted for the Vim, the Vce, the internal capsule and the globus pallidus, i.e. the regions where the stimulation is performed.

Accuracy improvements: With the use of a non-linear deformation function, the mapping of the atlas on the patient's MRI can be achieved with a good precision. Much of the remaining inaccuracy in the localization of the atlas onto the patient brain is caused by the geometrical distortions in the MRI image. Corrections of these distortions are currently under study and would be a central element for an increase in the localization accuracy of the atlas.

Registration improvements: The registration procedure used currently has been developed for general purposes, with a desire to obtain the best matching throughout the whole brain. For our particular needs, only a small region of the brain needs to be registered and certain anatomical characteristics, like the variability between two brains, could be relatively different from those

in the rest of the brain. By modifying certain parameters, the registration algorithm could be optimized to our specifications, resulting in hopefully a better registration accuracy, but above all, it could greatly reduce the computing time, passing from 6 hours to maybe less than 1 hour.

Bibliography

- [1] D. Albe-Fessard, G. Arfel, and G. Guiot. Activités électriques caractéristiques de quelques structures cérébrales chez l'homme. *Ann Chir*, 17:1185–1214, 1963.
- [2] N. Alpert, J. Bradshaw, D. Kennedy, and J. Correia. The principal axis transformation—a method for image registration. *Journal of Nuclear Medicine*, 31(10):1717, Octobre 1990.
- [3] J.A.V. Bates. The significance of tremor phasic units in the human thalamus. In F.J. Gillingham and I.M.D. Donaldson, editors, *Third symposium on Parkinson's disease*, pages 118–124, Edinbourg, London, 1969.
- [4] M. Bergström and T. Grietz. Stereotactic computed tomography. *American Journal of Roentgenology*, 127:167–170, 1976.
- [5] G. Bertrand, H. Jasper, A. Wong, and G. Mathews. Microelectrode recording during stereotactic surgery. *Clinical Neurosurgery*, 16:328–355, 1969.
- [6] Fred L. Bookstein. Principal warps: Thin-plate splines and the decomposition of deformations. *IEEE Transactions on Pattern Analysis and Machine Intelligence*, PAMI-11(6):567–585, 1989.
- [7] M. Brain. *Motif programming. The essentials... and more*. Digital Press, 1992.
- [8] D. L. Collins. *3D model-based segmentation of individual brain structures from magnetic resonance imaging data*. PhD thesis, McGill University, Montreal, Canada, 1994.

- [9] I. S. Cooper. *Parkinsonism-its medical and surgical therapy*, volume III. Thomas, Springfield, 1961.
- [10] J. Duchon. Interpolation des fonctions de deux variables suivant le principe de la flexion des plaques minces. *R.A.I.R.O., Analyse numérique*, 10:5–12, 1976.
- [11] A. C. Evans, W. Dai, D. L. Collins, P. Neelin, and T. Marrett. Warping of a computerized 3-d atlas to match brain image volumes for quantitative neuroanatomical and functional analysis. In *Proceedings of the international society of optical engineering; Medical imaging V*, San Jose, California, 27 February-1 March 1991. SPIE.
- [12] J. D. Foley, A. Dam, S. K. Feiner, and J. F. Hughes. *Computer graphics, principles and practice*. Addison-Wesley, 1990.
- [13] R. M. Gaze, F. J. Gillingham, S. Kalyanaraman, and A. A. Donaldson. Microelectrode recording from the human thalamus. *Brain*, 87:691–706, 1964.
- [14] R. Hassler. The influence of stimulation and coagulation in the human thalamus on the tremors at rest and its physiopathologic mechanism. In *Proceedings of the second international congress of neuropathology*, London, 1955.
- [15] C.J. Holmes, R. Hoge, D.L. Collins, and A.C. Evans. Posthoc enhancement of MR signal using automatic registration. In *2nd International Conference on Functional Mapping of the Human Brain*, page 240, Boston, June 1996.
- [16] V. Horsley and R.H. Clarke. The structure and functions of the cerebellum examined by a new method. *Brain*, 31:45–124, 1908.
- [17] G.N. Hounsfield, J. Ambrose, B.J. Perry, and C. Bridges. Computerized transverse axial scanning (tomography). *British Journal of Radiology*, 46:1016–1051, 1973.
- [18] M. Kilgard. *OpenGL Programming for the X Window system*. Addison-Wesley Developers Press, 1996.

- [19] L. Leksell. The stereotaxic method and radioscopy of the brain. *Acta Chir Scand*, 10:316–319, 1951.
- [20] L. Leksell. *Stereotaxis and radiosurgery: an operative system*. Charles C. Thomas, Springfield, Illinois, 1971.
- [21] L. Leksell and B. Jernberg. Stereotaxis and tomography. *Acta Neurochir.*, 52:1–7, 1980.
- [22] D.N. Levin, C.A. Pelizzari, G.T.Y. Chen, C.-T. Chen, and M.D. Cooper. Retrospective geometric correlation of MR, CT, and PET images. *Radiology*, 169:817–823, 1988.
- [23] D. McDonald. *Display - Program for display and segmentation of surfaces and volumes*. McConnell Brain Imaging Centre, Montreal, 1995.
- [24] R. Meyers. The modification of alternating tremors, rigidity and festination by surgery of the basal ganglia. *Res Pub Assoc Res Nervous Mental Disorders*, 21:602–665, 1942.
- [25] H. Narabayashi. *Tremor mechanisms*, chapter 32, pages 510–514. Georg Thieme Verlag, 1982.
- [26] K. Niemann, Ch. Naujokat, G. Pohl, C. Wollner, and D. v. Keyserlingk. Verification of the Schaltenbrand and Wahren stereotactic atlas. *Acta Neurochirurgica*, 129:72–81, 1994.
- [27] W. H. Press, B. P. Flannery, and W. T. vetterling S. A. Teukolsky. *Numerical recipes in C*. Cambridge University Press, Cambridge, 1988.
- [28] G. Schaltenbrand and P. Bailey. *Introduction to stereotaxis with an atlas of the human brain*, volume I. Georg Thieme Verlag, 1959.
- [29] G. Schaltenbrand and P. Wahren. *Atlas for stereotaxy of the human brain*, volume II. Georg Thieme Verlag, second edition, 1977.
- [30] M.C. Smith. Stereotaxic operations for Parkinson's disease and anatomical observations. *Mod trends Neurol*, 4:21–52, 1951.

- [31] E.A. Spiegel and H.T. Wycis. *Stereoencephalotomy(thalamotomy and related procedures)*, volume Part 1. Grune, New York, 1952.
- [32] E.A. Spiegel, H.T. Wycis, and M. Marks. Stereotaxic apparatus for operations on the human brain. *Science*, 106:349–350, 1947.
- [33] J. Talairach, H Hecaen. M. David, and J. Ajuriaguerra M. Monnies. Recherches sur la coagulation thérapeutique des structures souscorticales chez l’homme. *Rev neurol*, 81:4–24, 1949.
- [34] J. Talairach, M. David, P. Tournoux, H. Corredor, and T. Kvasina. *Atlas d’Anatomie Stéréotaxique*. Masson et Cie, Paris, 1957.
- [35] A. E. Walker. *Classification of movement disorders*, chapter 33, pages 515–521. Georg Thieme Verlag, 1982.
- [36] A. E. Walker. *Classification of movement disorders*, chapter 31, pages 503–509. Georg Thieme Verlag, 1982.